THERMO 2023

RIVA DEL GARDA

PRE-CONFERENCE FIELD TRIP

31st August – 3rd September 2023

Field leaders:

Marco G. Malusà and Stefano Zanchetta

(University of Milano-Bicocca)

Day 1: Meeting in Brixen – Introduction

Day 2: The Insubric Fault

Day 3: The Tauern Window and the Brenner Normal Fault

Day 4: The Southalpine domain of the western Dolomites

Day 1 (Thursday 31st August)

Meeting in Brixen - Introduction

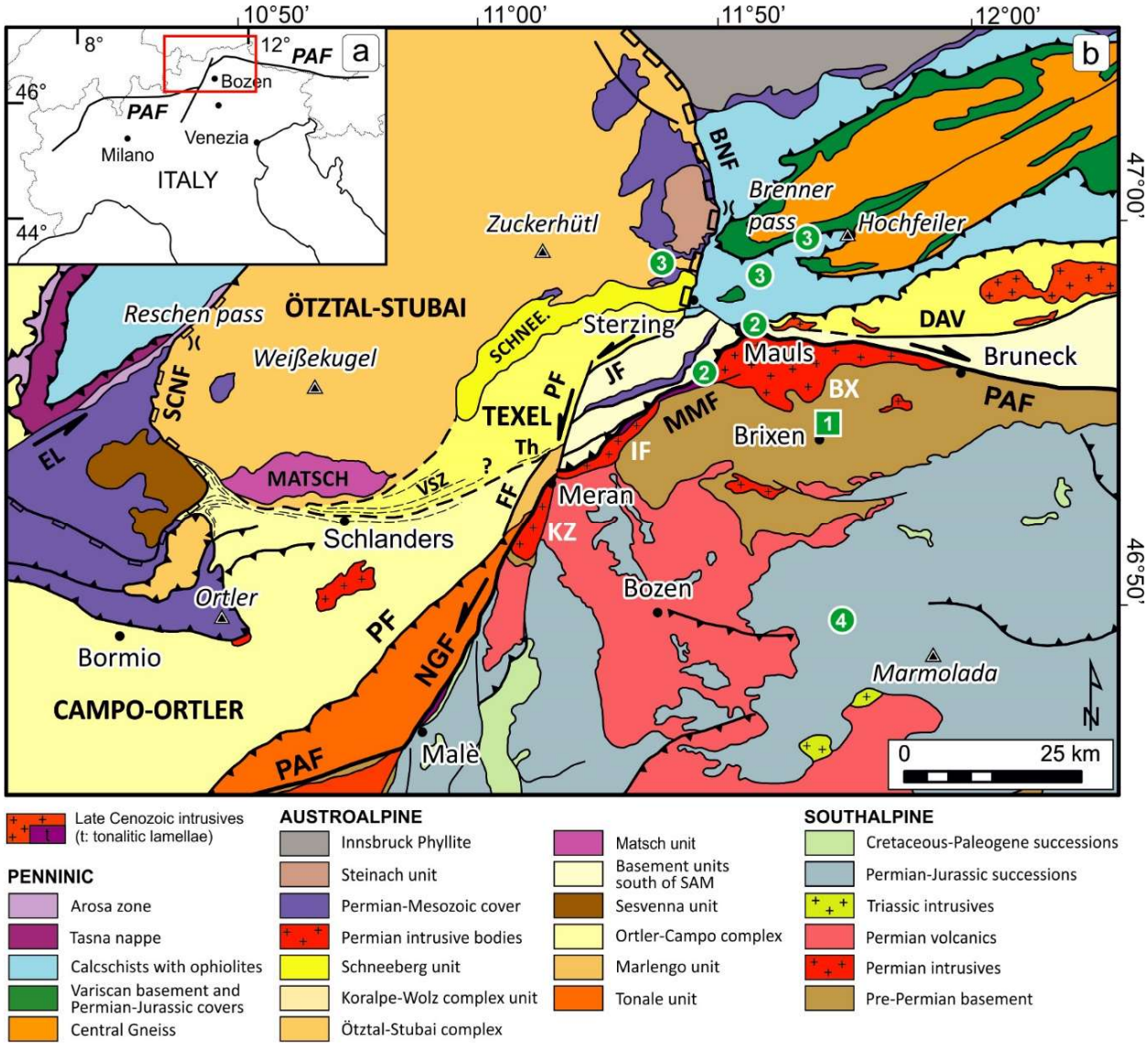

Figure 1.1: Tectonic sketch map of the Periadriatic Fault (PAF) from the Adamello area to the western Tauern Window. Numbers in green indicate the days of the field trip. The Meran-Mauls segment (MMF) extends in the central part of the figure from the town of Meran (SW) to Mauls (NE). BNF: Brenner Normal Fault; BX: Brixen granodiorite; DAV: Defereggen-Anthoslz-Vals Fault; EL: Engadine Line; IF: Ifinger granodiorite; JF: Jaufen Fault; KZ: Kreuz Spitze granite; NGF: North Giudicarie Fault; PF: Passeier Fault; PJ: Pejo Fault; SCNF: Schlinig Normal Fault; VSZ: Vinschgau Shear Zone (after Zanchetta et al. 2023).

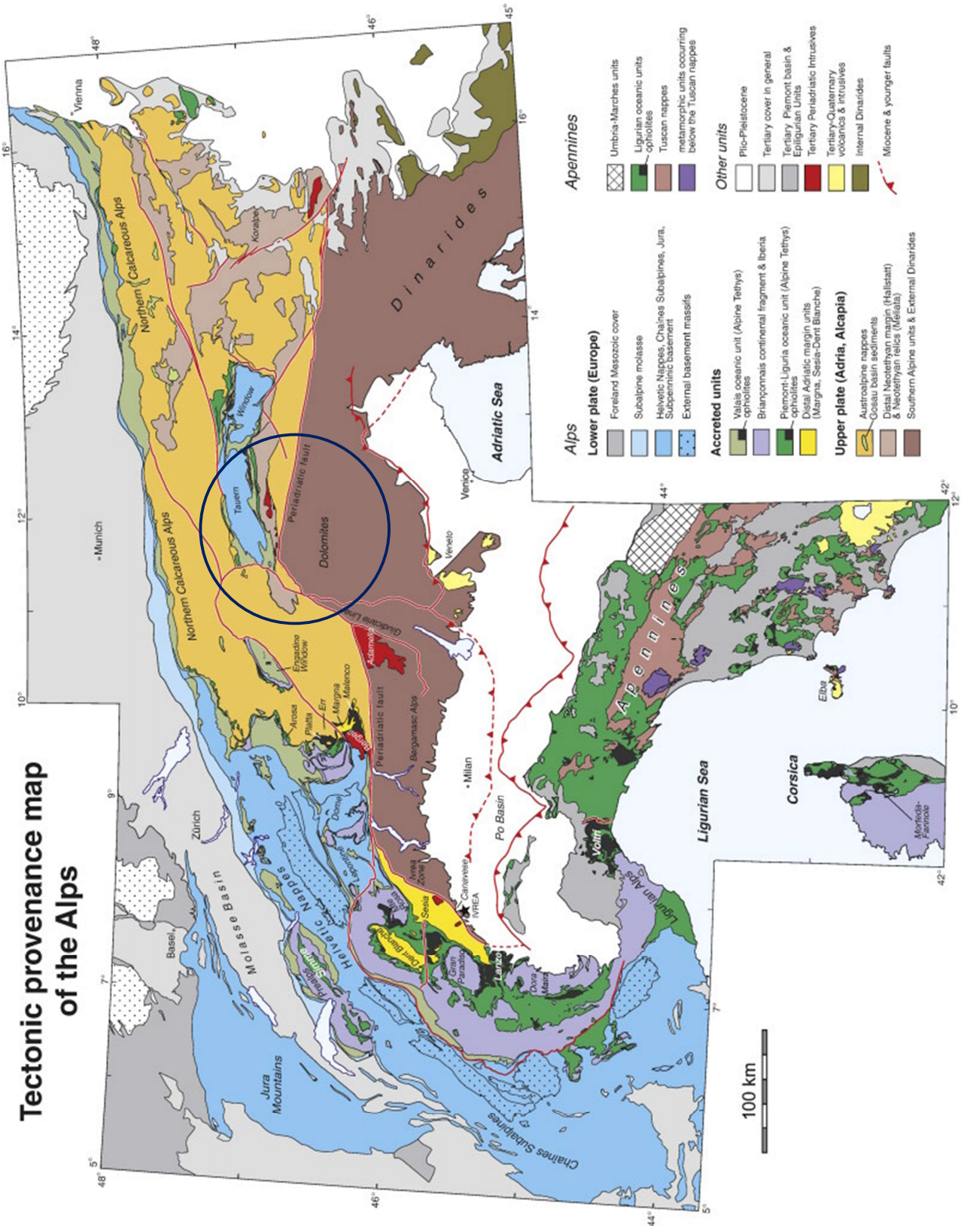

Figure 1.2: Tectonic map of the Alps (Handy et al. 2010). Blue circle = area analyzed during the field trip

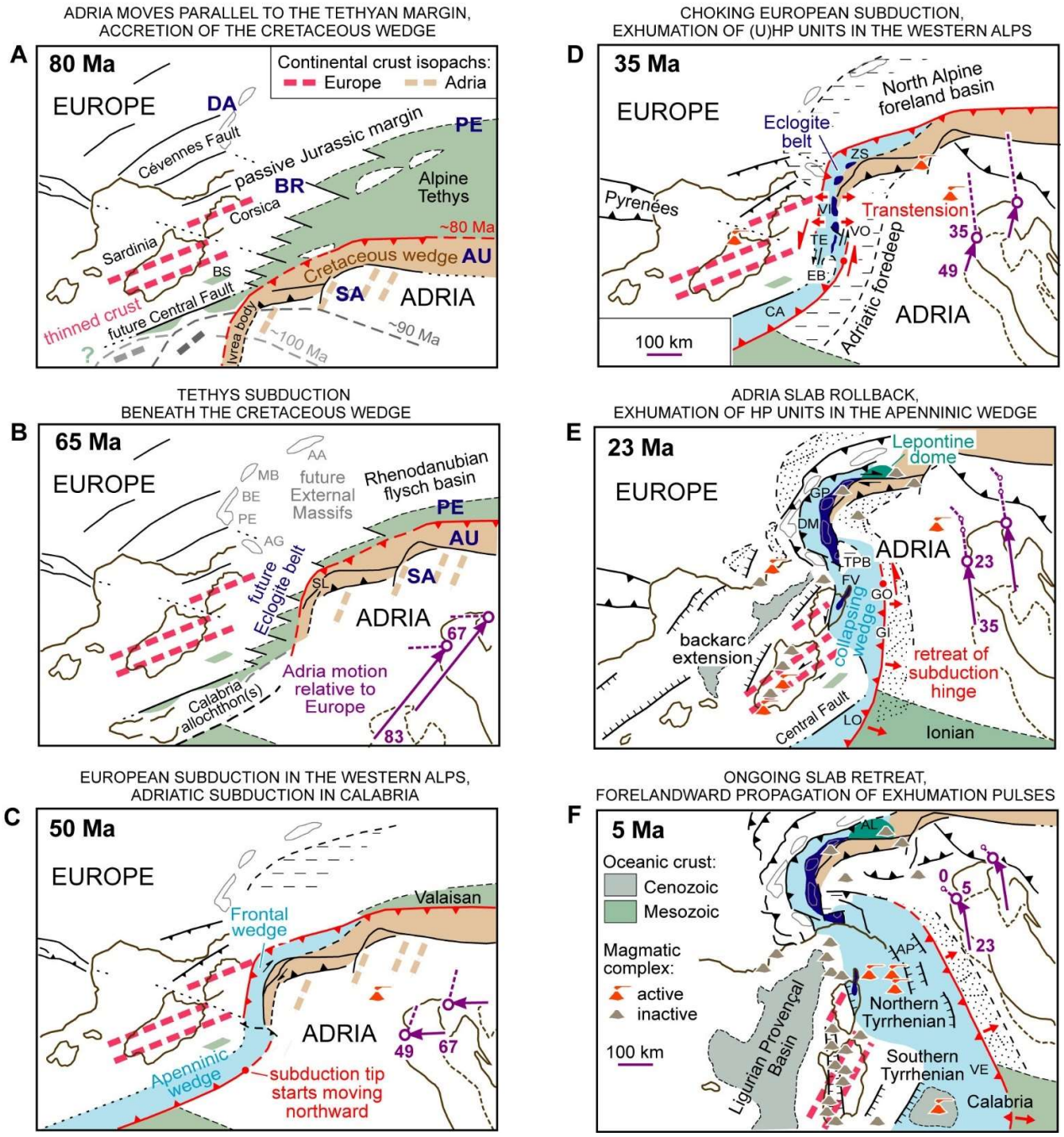

Figure 1.3: Evolution of the Alps-Apennines system since the Cretaceous (Malusà et al. 2015); Adria trajectories relative to Europe from Dewey et al. (1989) Active subduction zones are marked in red. Blue acronyms in bold: AU = Austroalpine; SA = Southalpine; PE = Penninic; BR = Brianconnais; DA = Dauphinoise. Other smaller acronyms: AA, Aar; AL, Alpe Arami; AP, Apuane; AR, Argentera; BE, Belledonne; BS, Baronie Smt; CA, Castagna; DM, Dora-Maira; EB, Epiligurian basins; FV, Farinole-Volpajola; GI, Giglio; GO, Gorgona; GP, Gran Paradiso; LO, Gimigliano lower ophiolites; VE, Lungro-Verbicaro; MB, Mont Blanc; PE, Pelvoux; SL, Sesia-Lanzo; TE, Tenda; TPB, Tertiary Piedmont Basin; VI, Viso; VO, Voltri ZS, Zermatt-Saas.

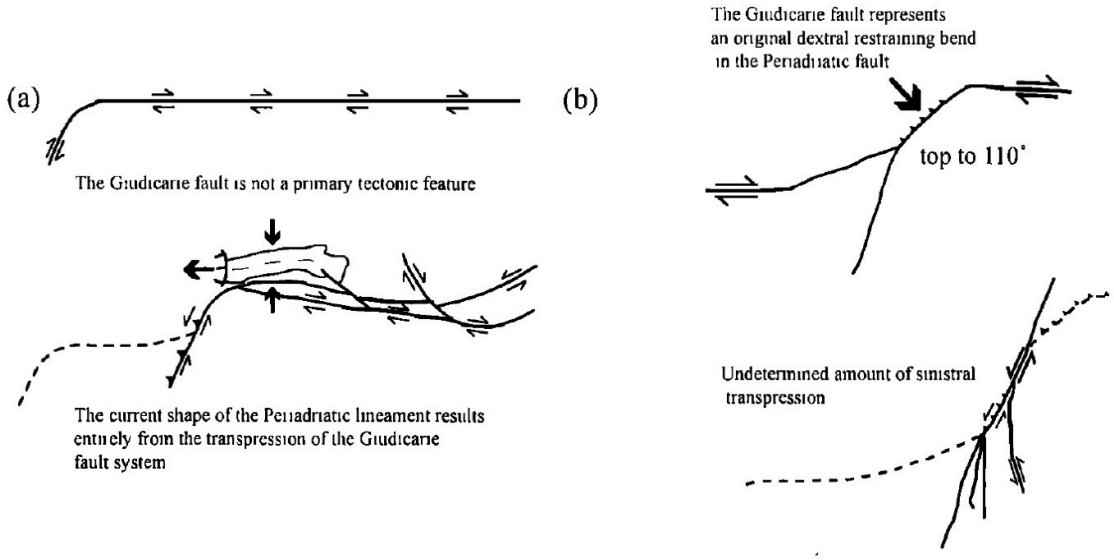

Figure 1.4: Possible alternative kinematic models for the Giudicare fault system. (a) the Giudicarie fault system is not a primary tectonic feature; (b) the Giudicarie fault system is an original dextral restraining bend in the Periadriatic fault. Solid lines are active faults. Dashed lines are inactive fault segments (from Viola et al. 2001).

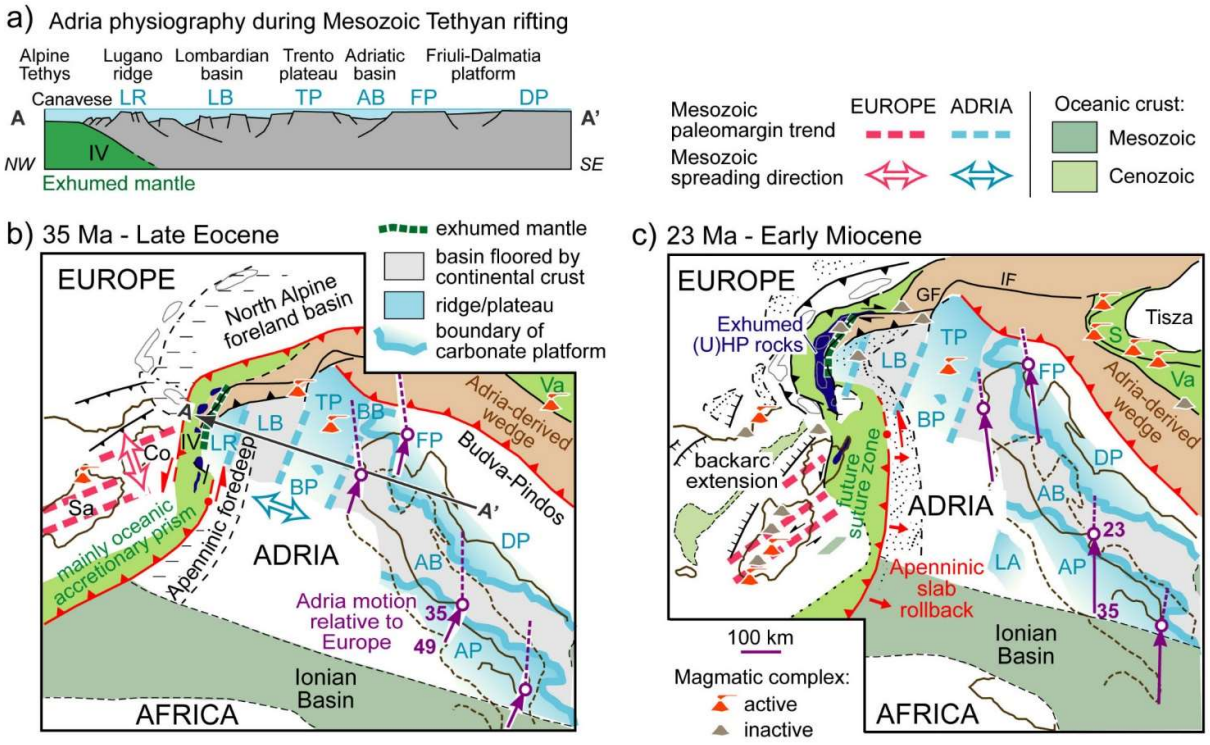

Figure 1.5: a) Extensional architecture of the Adriatic microplate during Tethyan rifting, 2×vertical exaggeration, see location of cross-section in frame (b) (based on Winterer and Bosellini, 1981; Bertotti et al., 1993). (b)–(c)Palinspastic reconstruction of the Adria–Europe plate boundary zone during Eocene (U)HP rock exhumation in the Western Alps (b) and the onset of Apenninic slab rollback (c). Purple arrows indicate Adria–Europe relative plate motion (numbers = age in Ma) (from Sun et al. 2019).

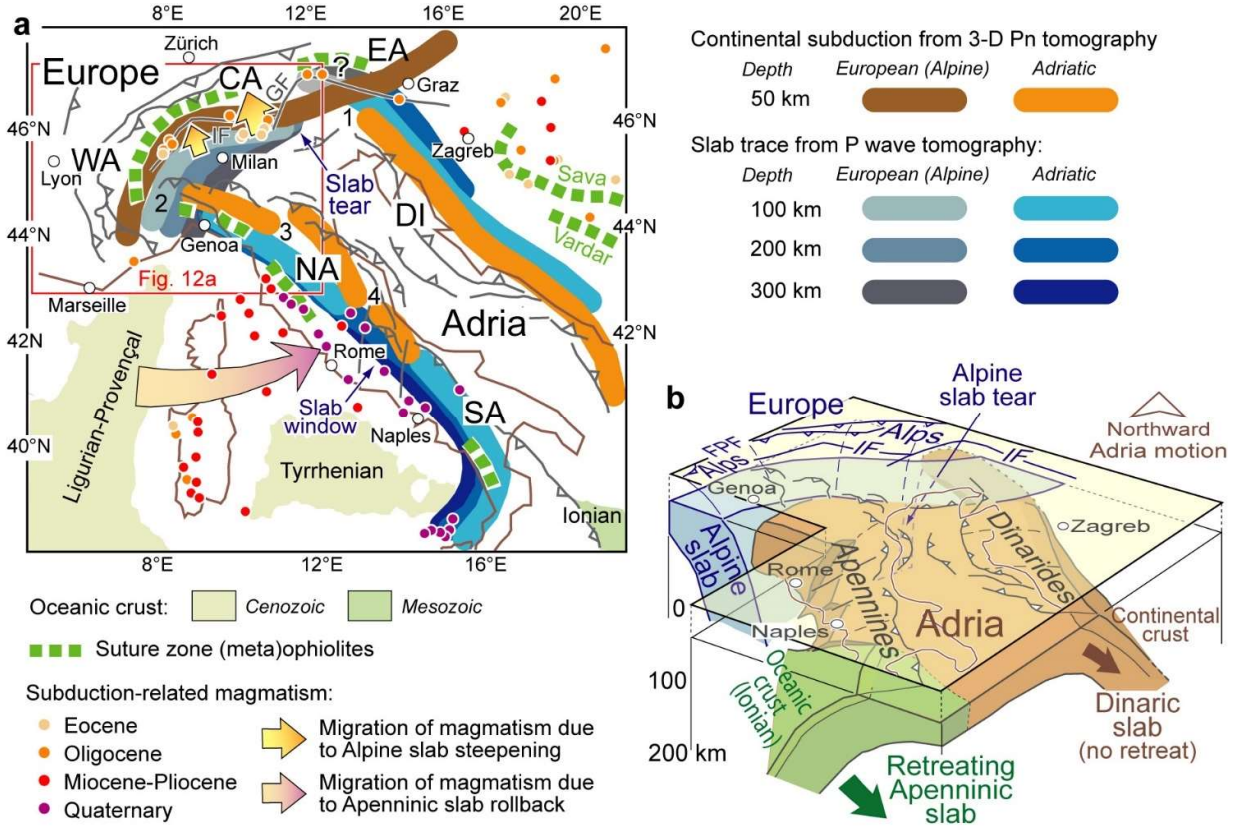

Figure 1.6: Interpretive slab structure beneath the Alpine region as constrained by recent tomography studies (from Malusà et al. 2021). (a) Tectonic sketch map showing the relations among slab structure, distribution of orogenic magmatism and accreted (meta)ophiolites. The present-day slab traces at 100, 200, and 300-km depth are based on the P-wave tomography models of Zhao et al. (2016) and Piromallo and Morelli (2003). The question mark indicates the controversial high-velocity anomaly beneath the remnants of the former Alpine subduction zone (b) Cartoon summarizing the relationships between the Alpine slab and the Apenninic and Dinaric slabs.

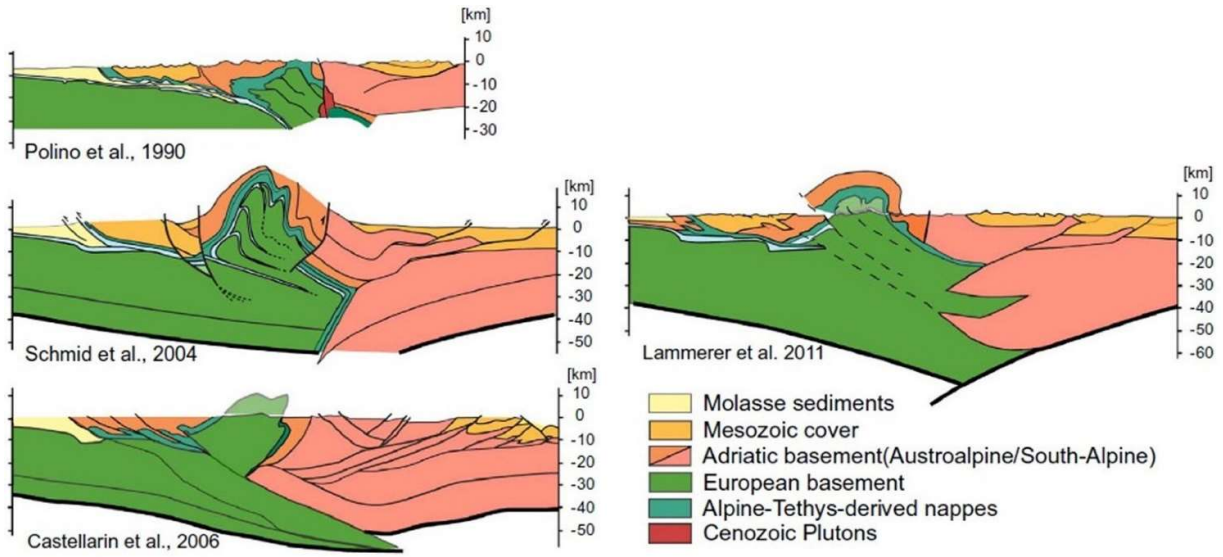

Figure 1.7: Deep structure of the Eastern Alps as interpreted by different authors (from Rosenberg et al. 2018).

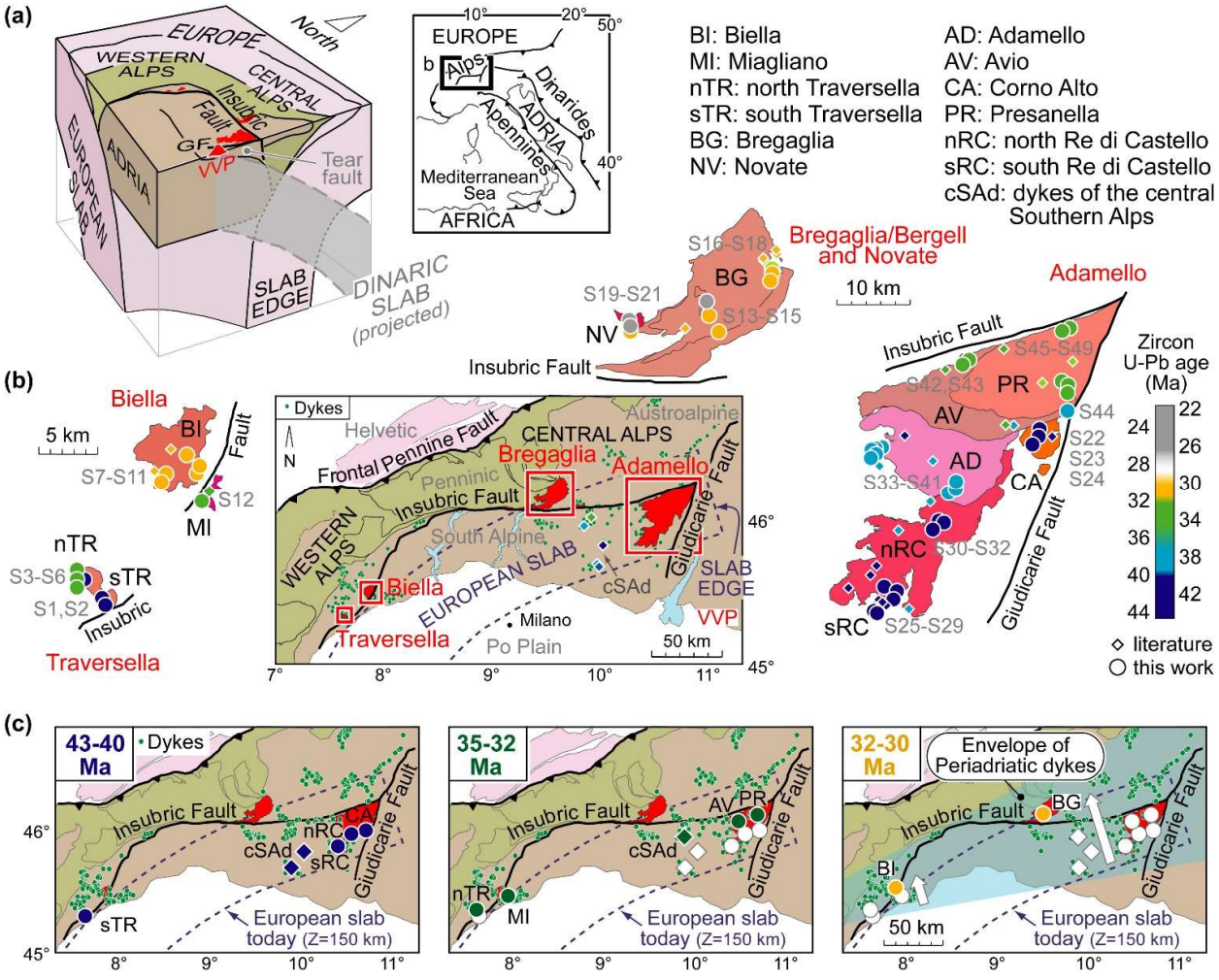

Figure 1.8: A: Relationships between tectonic structure and Periadriatic magmatism in the Western and Central Alps (Ji et al. 2019). GF = Giudicarie Fault; VVP = Venetian Volcanic Province. B: Summary of weighed mean 206Pb-238U zircon ages in the western Periadriatic intrusives. C: Migration of Periadriatic magmatism in three steps (43-40, 35-32 and 32-30 Ma) and relationships with the European slab as outlined by seismic tomography (Zhao et al., 2016). White arrows = younging trends defined by zircon U-Pb ages.

Pluton	Unit	Sample	Zircon U-Pb ages (Ma)		εHf(t)	
			*this work**	*literature***	*this work*	*literature*
Traversella	sTR	S1, S2	42-41	-	-7.8 / -1.1	-
	nTR	S3-S6	33 (41)	-	-8.0 / -3.1	-
Biella	MI	S12	33	33	-5.2 / -1.3	-
	BI	S7-S11	31-30 (30)	31-30	-8.0 / -1.8	-
Adamello	CA	S22-S24	43	42	+2.6 / +10.8	-
	RCm	S28-S29	41	43-40	+9.0 / +13.9	+4.7 / +14.4
	sRC	S25-S27	43	43-41	+2.1 / +9.0	-0.4 / +11.4
	nRC	S30-S32	41	39-38	-8.8 / +7.0	-
	AD	S33-S41	38-37 (40, 38)	42-37	-9.6 / +6.7	-
	AV	S42-S44	36-34 (34)	36-33	-10.0 / -3.2	-
	PR	S45-S49	34-33	32	-8.5 / -2.8	-
Bregaglia	BGm	-	-	31	-	+1.6 / +5.5
	BG	S13-S18	32-30 [25]	32-30	-7.6 / -2.0	-
	NV	S19-S21	27-24 (32)	24	-8.5 / -0.3	-

* sample mean ages (data in round brackets are for mafic enclaves and in squared brackets for dykes). ** see references Ji et al. (2019).

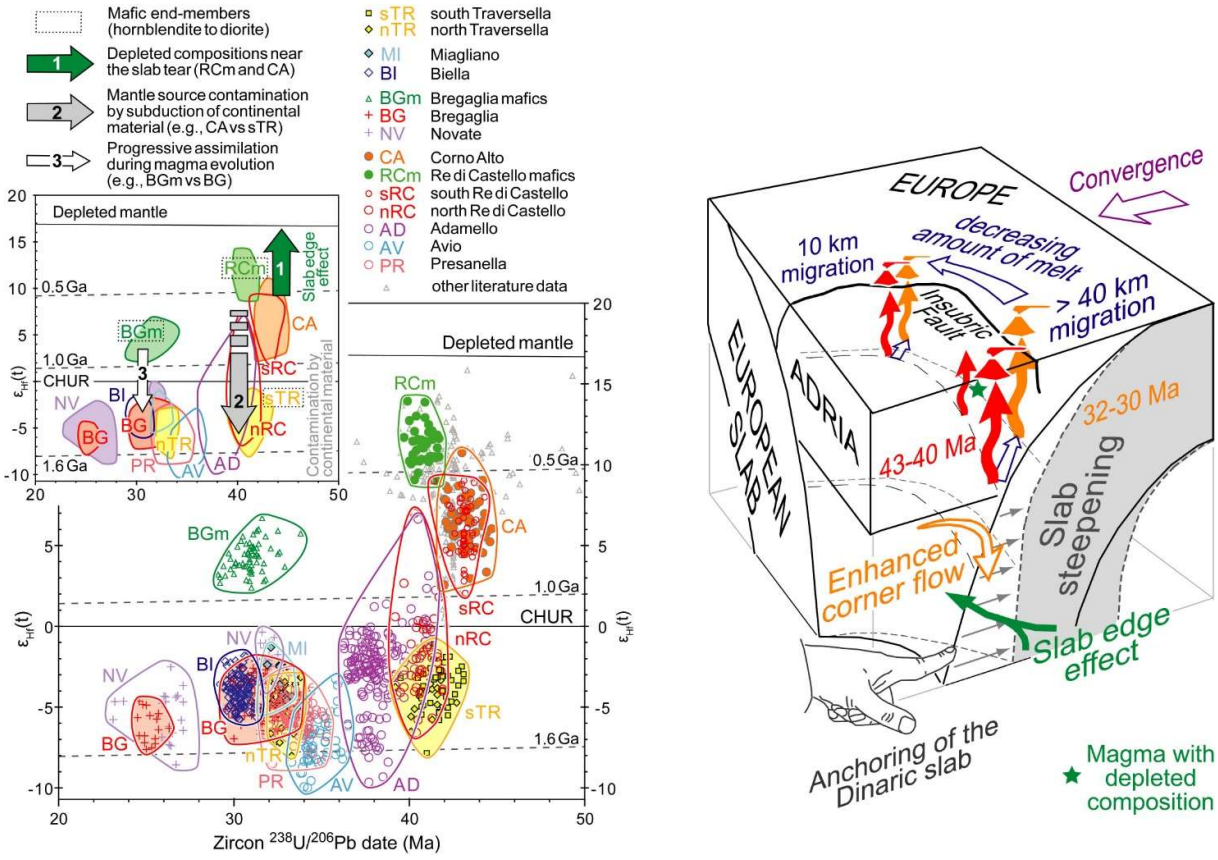

Figure 1.9: On the left: Single zircon ^{206}Pb-^{238}U dates and Hf isotope compositions from the main Periadriatic intrusions of the Western and Central Alps. The field for the Bregaglia mafic rocks is after Tiepolo et al. (2014); literature data from the Re di Castello unit (small grey triangles) are from Schoene et al. (2012) and Broderick et al. (2015). The inset on the top-left summarizes the main trends discussed in the text. Note the systematic εHf(t) decrease from east to west in the mafic end-members (RCm, BGm and sTR) (from Ji et al. 2019).

On the right: 3-D model showing the relationships between slab steepening and Periadriatic magmatism in the absence of slab breakoff as proposed by Ji et al. (2019). Slab steepening enhances the corner flow, more asthenospheric material is involved in source partial melting thus triggering magmatism. This process is more effective in the Central Alps (right side of the model) because of (i) the free boundary represented by the slab edge, (ii) the anchoring of the Dinaric slab that may have pushed back the European slab, and (iii) a minor amount of buoyant continental crust subducted at the trench. Migration of magmatism (10 km in the Western Alps, >40 km in the Central Alps) is based of Fig. 1.8C and on plutons only. The estimate for the Central Alps is conservative and may increase for greater amounts of dextral strike-slip accommodated along the Insubric Fault. Magmas with depleted compositions (green star) are generated in the vicinity of the torn edge of the European slab, due to the greater contributions of juvenile components during source melting (slab edge effect in the cartoon).

Day 2 (Friday 1st September)

The Insubric Fault near Pennes Pass

Near Pennes Pass, Austroalpine paragneiss of Variscan age are thrusted on the Lower Permian Brixen Granodiorite that is intruded into Southalpine rocks.

Oligocene Tonalites are sheared as tectonic slices within the fault zone. In the morning, the bus will take us to Pennes Pass (2210 m asl), where we will start walking along a scenic mountain path with slight elevation gain carrying out a series of geological observations. We will cross the mylonites and cataclasites of the Periadriatic Fault System, the kyanite-bearing paragneiss and the Permian-Triassic sediments of the Austroalpine domain exposed to the north of the fault, and the lower Permian Brixen granite of the Southalpine domain exposed to the south of the fault. We will discuss available thermochronological data to constrain the fault activity, and we will enjoy the wonderful panoramas towards the Tauern window to NE, the Dolomites to SE, and the Calcareous Alps and the Oetztal Nappe with its Permian-Triassic cover rocks to NW. We will have our lunch near the pass, and, in the afternoon, the bus will take us down in the valley to observe the Permian-Triassic sediments of the Pens-Stilves-Weisshorn unit at Mauls (Mules).

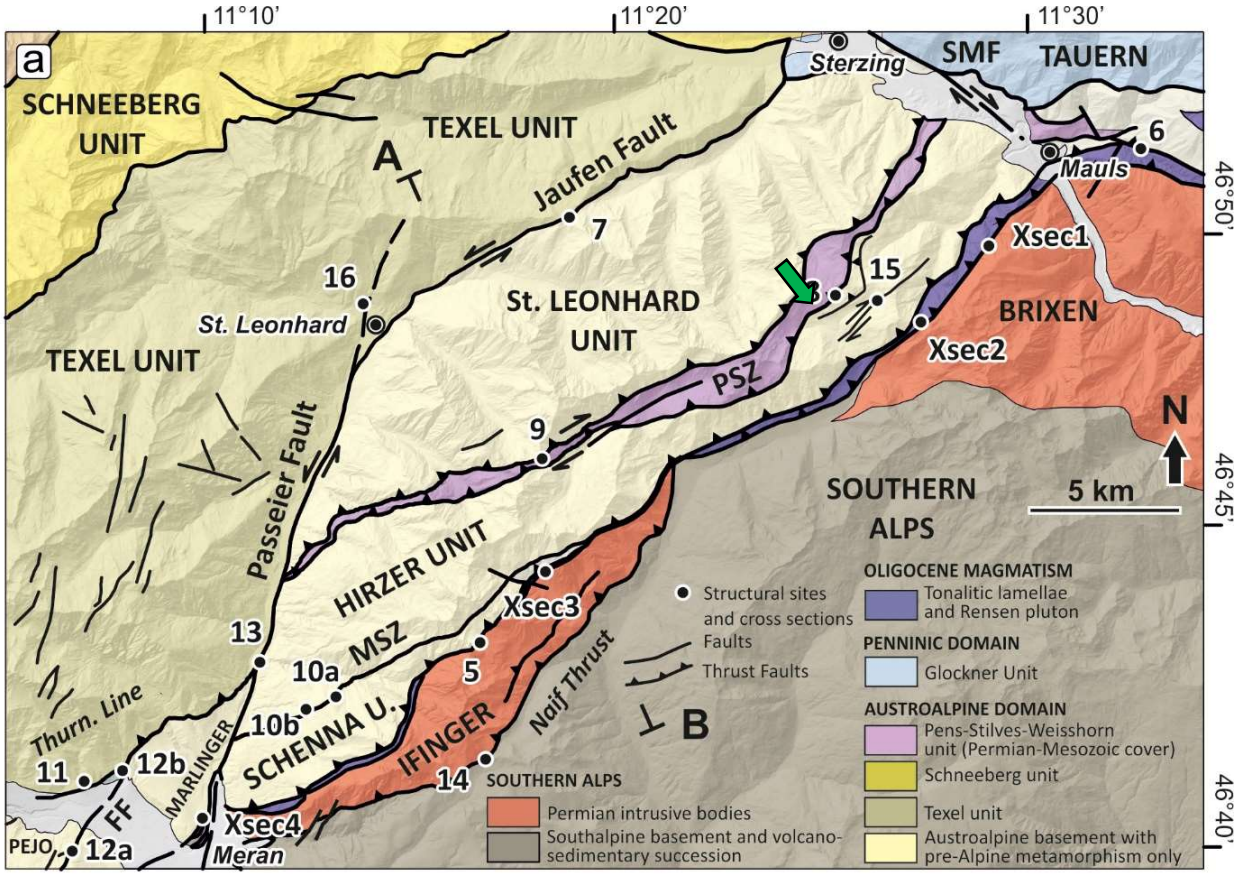

Figure 2.1: Tectonic map of the Insubric Fault around Pennes Pass (Meran-Mauls fault segment). The green arrow marks the analyzed section. FF: Forst Fault; MSZ: Masul Shear Zone; PSZ: Pens Shear Zone (from Zanchetta et al. 2023).

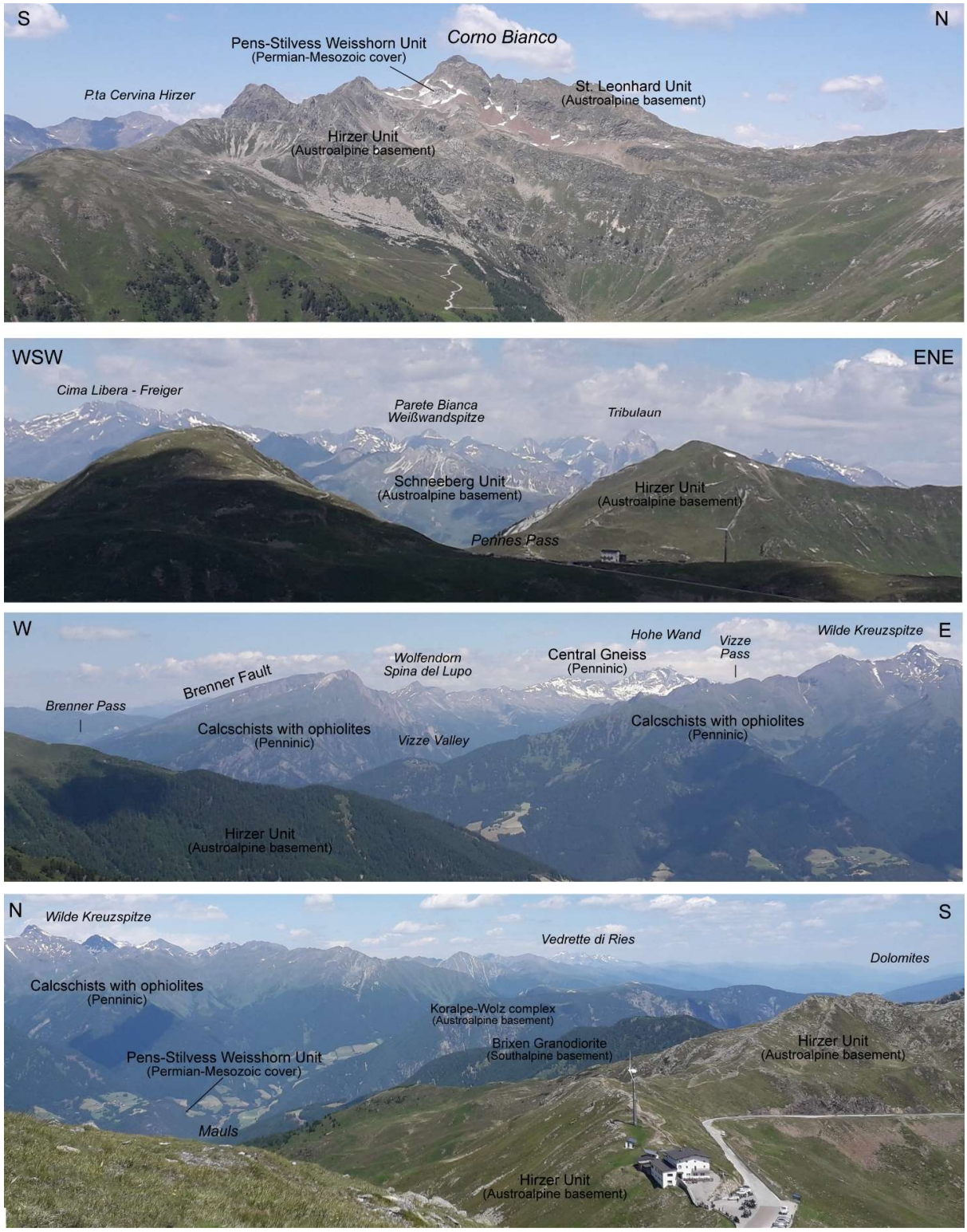

Figure 2.2: Main geological features of the Austroalpine and Penninic domains in the landscape around Pennes Pass.

Figure 2.3 (next page): The Insubric Fault in the landscape around Pennes Pass.

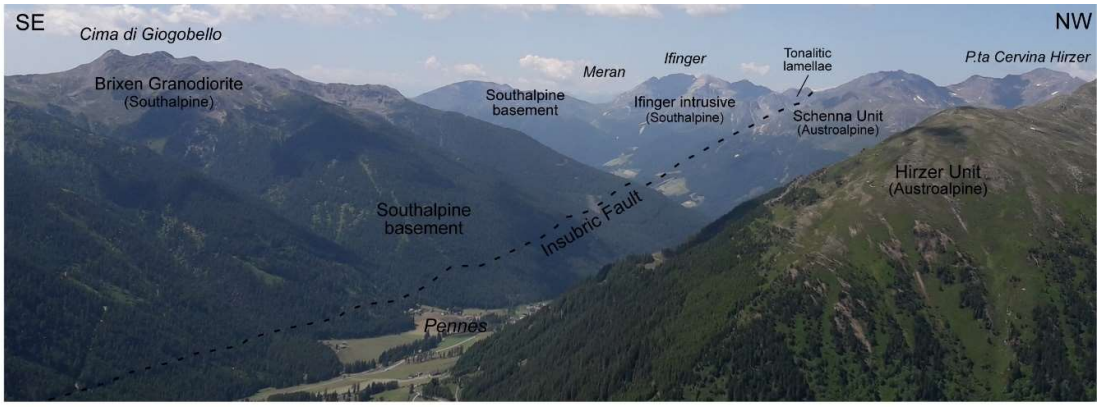
SE
NW
Cima di Giogobello
Brixen Granodiorite
(Southalpine)
Meran
Ifinger
Tonalitic
lamellae
P.ta Cervina Hirzer
Southalpine
basement
Ifinger intrusive
(Southalpine)
Schenna Unit
(Austroalpine)
Hirzer Unit
(Austroalpine)
Southalpine
basement
Insubric Fault
Pennes

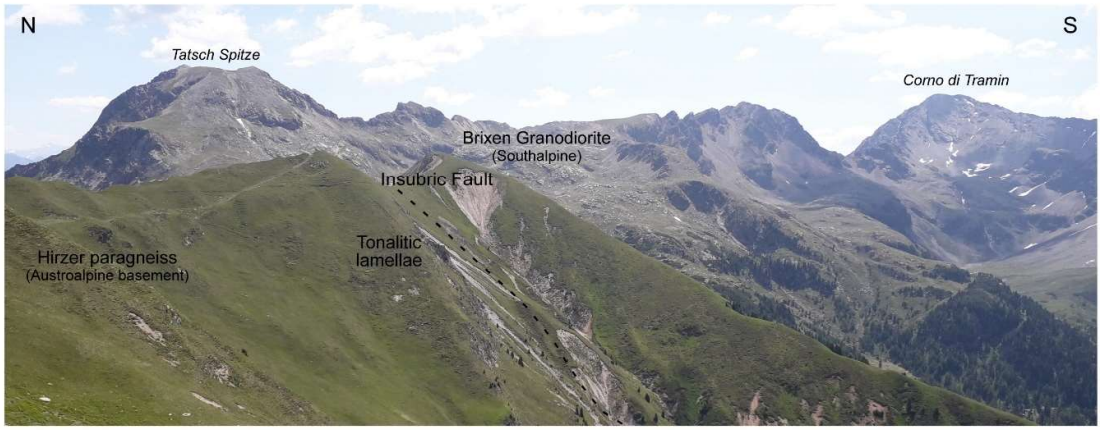
N
S
Tatsch Spitze
Corno di Tramin
Brixen Granodiorite
(Southalpine)
Insubric Fault
Tonalitic
lamellae
Hirzer paragneiss
(Austroalpine basement)

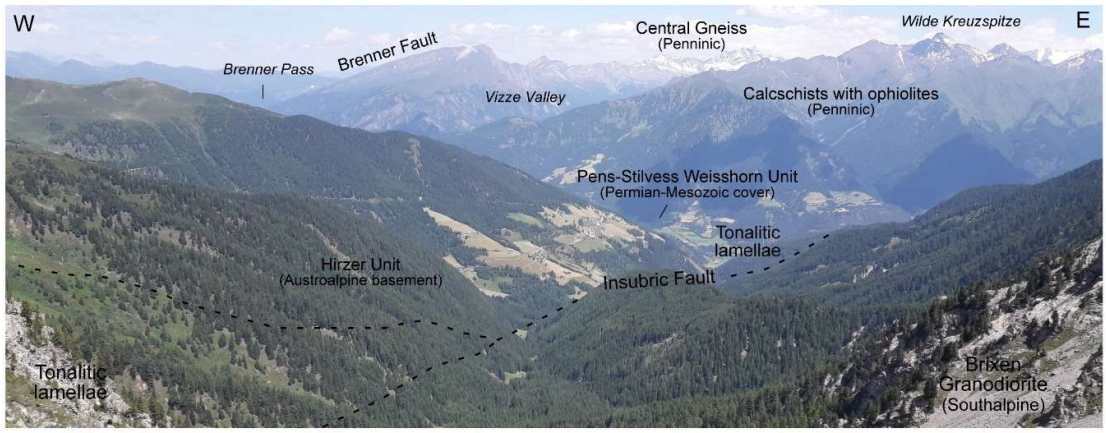
W
E
Brenner Pass
Brenner Fault
Central Gneiss
(Penninic)
Wilde Kreuzspitze
Vizze Valley
Calcschists with ophiolites
(Penninic)
Pens-Stilvess Weisshorn Unit
(Permian-Mesozoic cover)
Tonalitic
lamellae
Hirzer Unit
(Austroalpine basement)
Insubric Fault
Tonalitic
lamellae
Brixen
Granodiorite
(Southalpine)

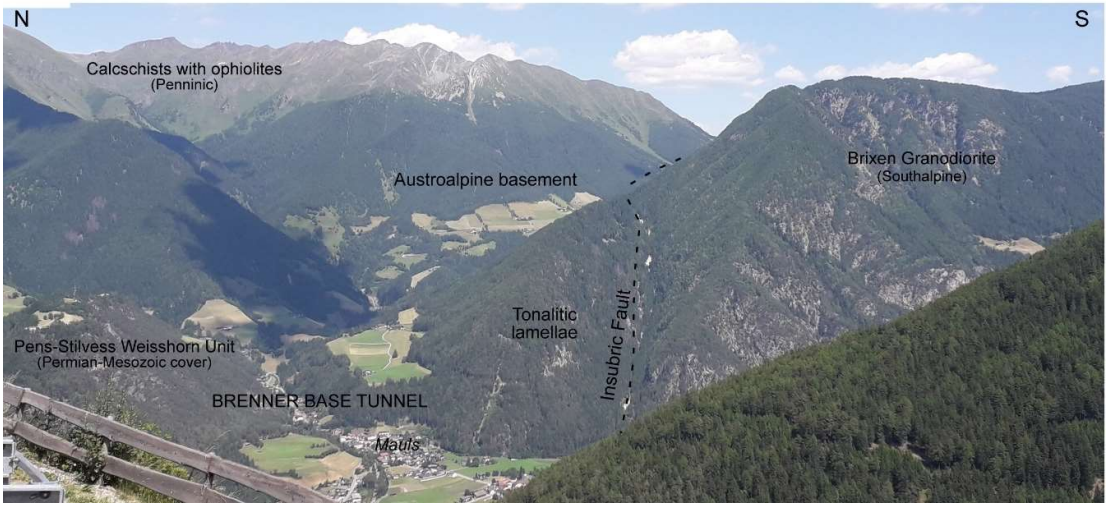
N
S
Calcschists with ophiolites
(Penninic)
Austroalpine basement
Brixen Granodiorite
(Southalpine)
Tonalitic
lamellae
Insubric Fault
Pens-Stilvess Weisshorn Unit
(Permian-Mesozoic cover)
BRENNER BASE TUNNEL
Mauls

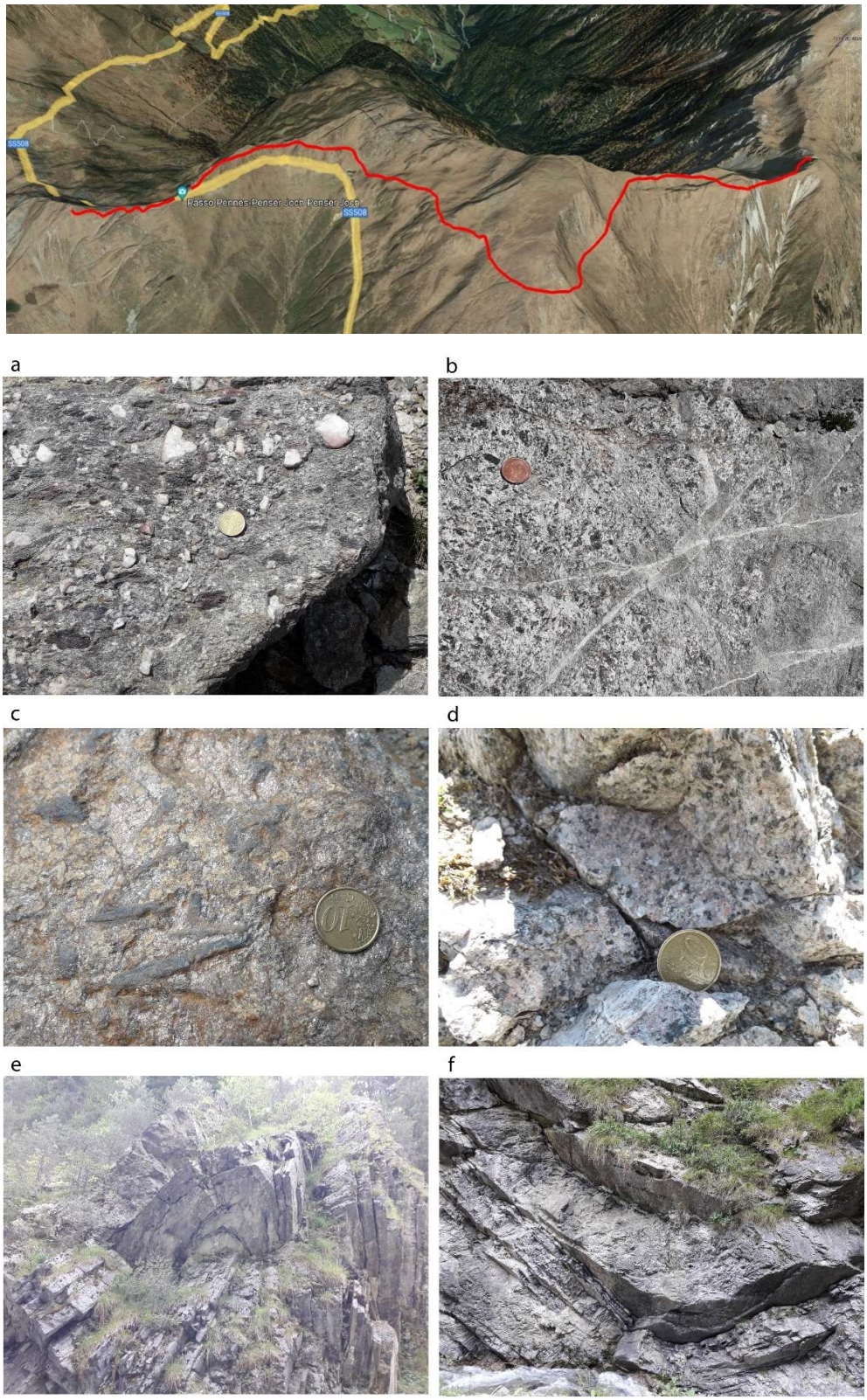

Figure 2.4: a) Permian conglomerate ("Verrucano di Mules" Auct.), Austroalpine domain; b) Tonalite with cataclastic shear bands, Periadriatic magmatism; c) Kyanite-bearing paragneiss of the Hirzer unit, Austroalpine domain; d) Brixen Granodiorite (Southalpine domain); e,f) Mesozoic cover sequence of the Pens-Stilves-Weisshorn Unit near Mules.

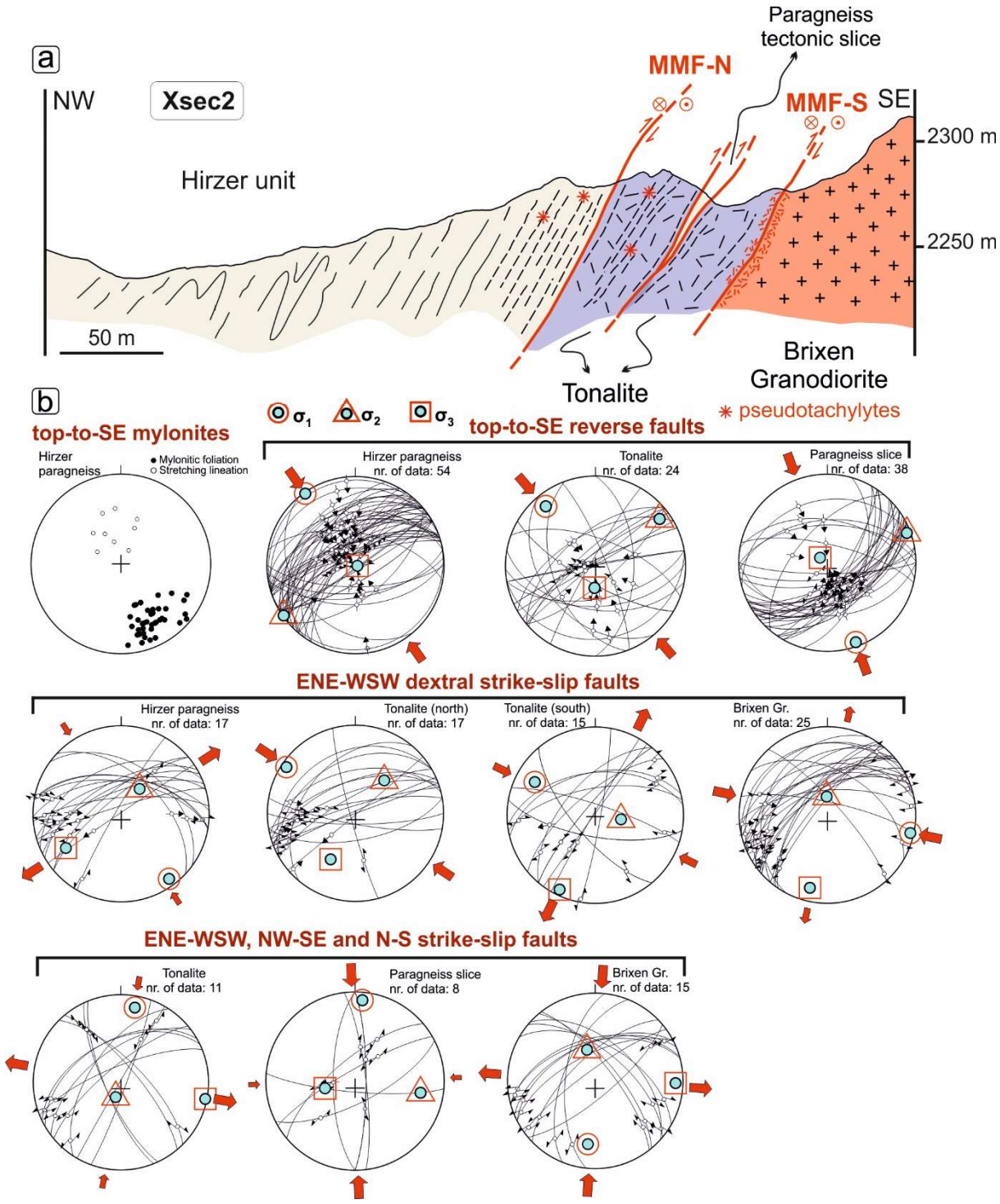

Figure 2.5: Cross section Xsec2 across the Insubric Fault (Meran-Mauls fault segment) to the E of Pennes Pass. (b) top-to-SE mylonites (stage 1) occur in the Hirzer unit paragneiss close to the faulted contact with the tonalite, whereas only minor ductile shear bands occur in the tonalites. The overprinting brittle deformation consists in at least three different deformation stages that pass from top-to-SE thrusting (stage 2), to dextral transpression (stage 3), and final N-S compression with subvertical conjugate strike-slip fault systems (stage 4) (from Zanchetta et al. 2023).

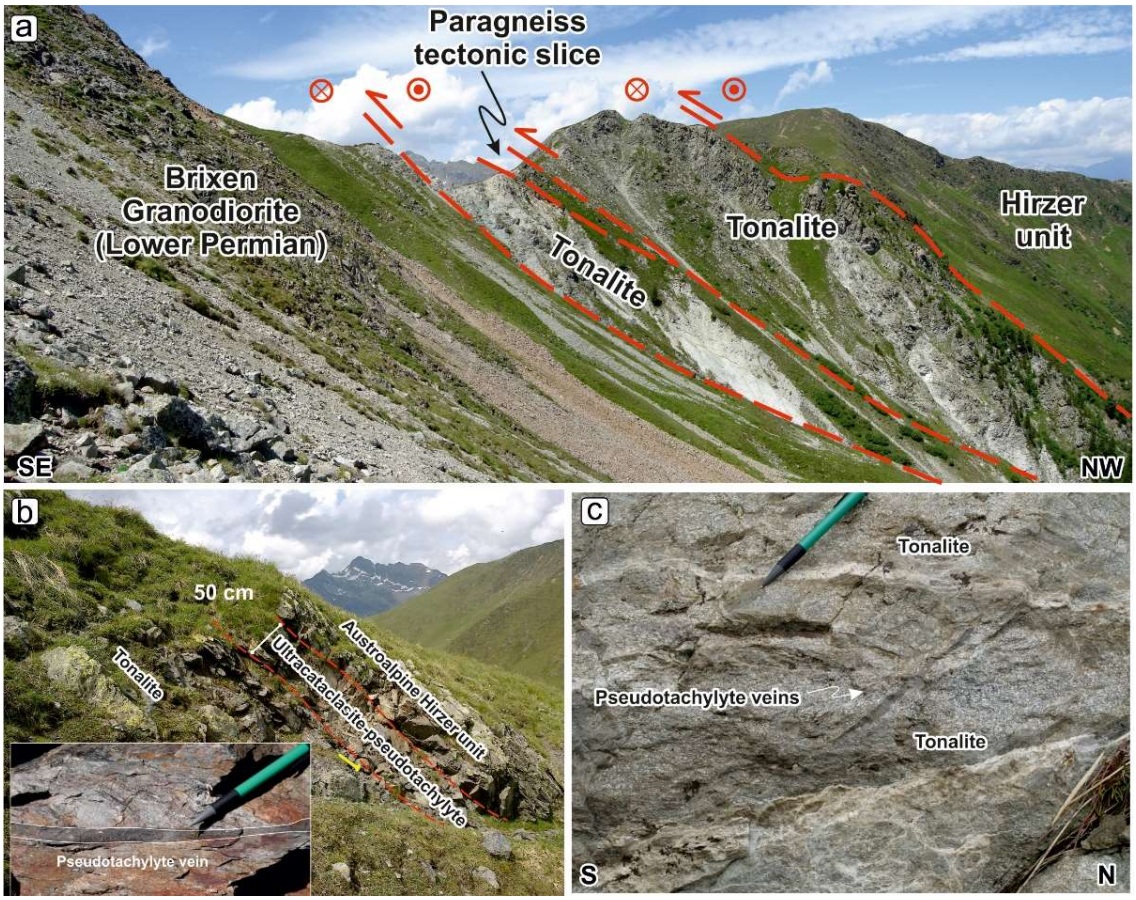

Figure 2.6: (a) panoramic view towards the Meran-Mauls fault segment from the path leading to Pennes Pass. (b) pseudotachylytes-bearing ultracataclastic bands overprinting mylonites of the Hirzer unit. (c) another panoramic view of the Meran-Mauls fault segment with cataclasites derived from the tonalitic lamella (from Zanchetta et al. 2023).

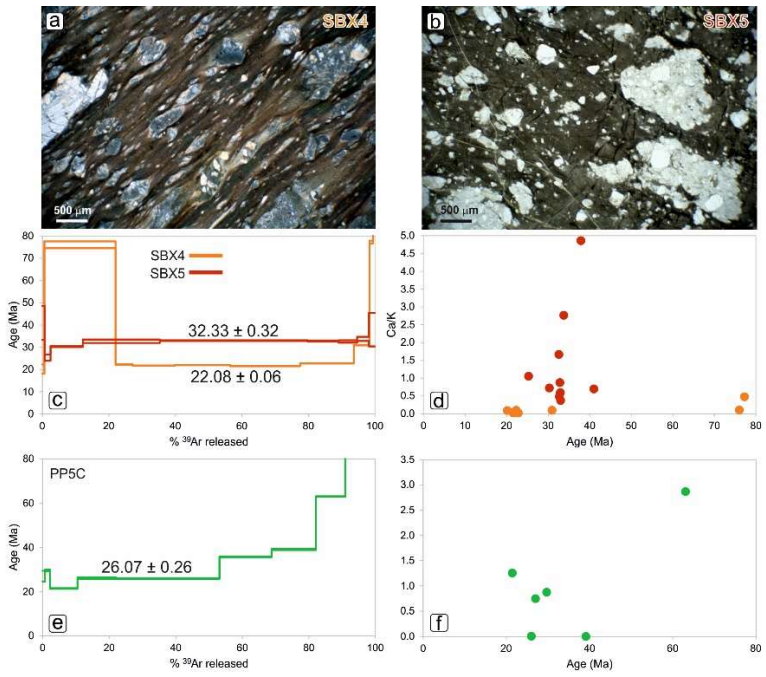

Figure 2.7: $^{40}Ar/^{39}Ar$ spectra vs age correlation diagrams. (a) undeformed pseudotachylyte veins, sample SBX5. (b) sheared peseudotachylyte, sample SBX4. (c) $^{40}Ar/^{39}Ar$ spectra of sample SBX4, orange (Xsec4), and SBX5, red (same site). (d) Ca/K diagram for samples of figure (c). (e) 40Ar/39Ar spectrum of a pseudotachylyte from Niedereck (Xsec2, Fig. 2) and (f) associated Ca/K vs age diagram (from Zanchetta et al. 2023).

Figure 2.8: Evolution of the Meran-Mauls Fault from activation to post-Miocene times. (a) top-to-SE thrusting at ductile conditions is recorded by mylonites in the Austroalpine hanging wall and, locally, tonalites and the Lower Permian granitoids in the footwall. The maximum age is constrained by the gabbro lens of Weissbach (38.9 Ma). (b) top-to-SE thrust faults overprinted mylonites all along the MMF. The maximum age of this stage is provided by the 22.1 Ma age of the ductile deformed pseudotachylyte at Zenoberg. (c) dextral strike-slip to transpressive reactivation of older structures mainly occur in the NE segments of the MMF and along the Pens Shear Zone, whereas no evidence of this stage is observed at the SW termination of the MMF. (d) the end of dextral shearing along the MMF is provided by the activation of subvertical strike-slip faults related to N-S compression. A pseudotachylyte age of 17 Ma along the Passeier Fault likely constrain the onset of this deformation stage (from Zanchetta et al. 2023).

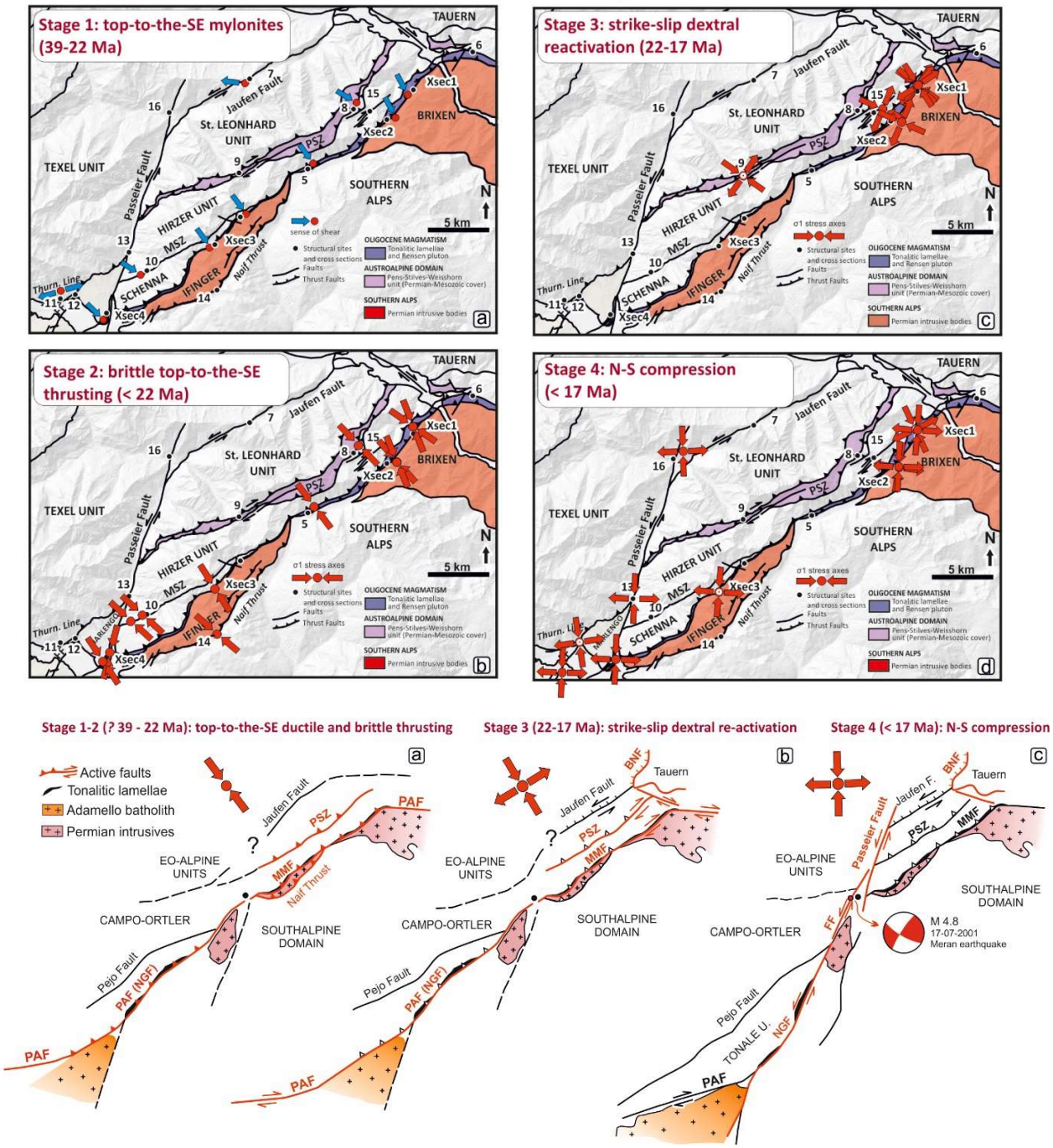

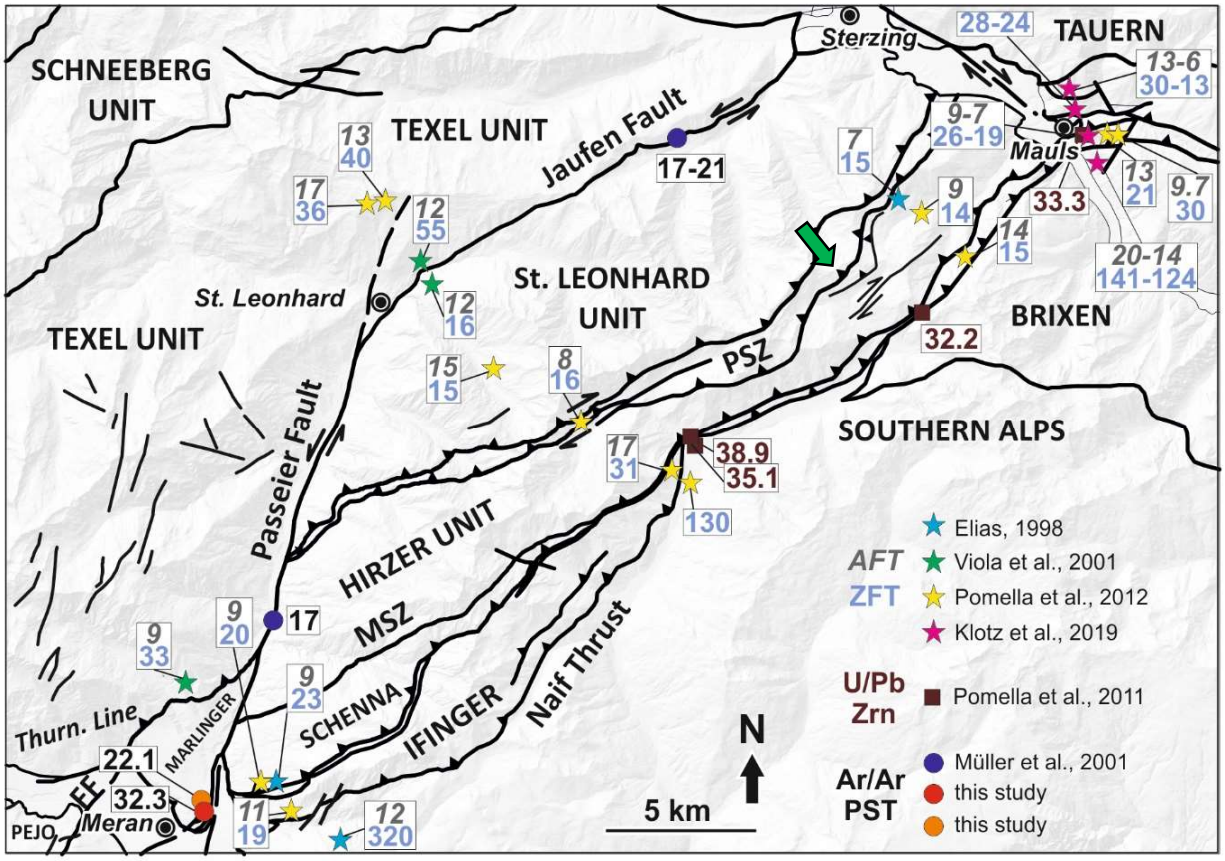

Figure 2.9: Compilation of geochronological and thermochronological data (from Zanchetta et al. 2023). The green arrow marks the analyzed section.

Figure 2.10: Simplified stratigraphic column of the Permian-Triassic sediments of the Pens-Stilves-Weisshorn unit at Mauls.

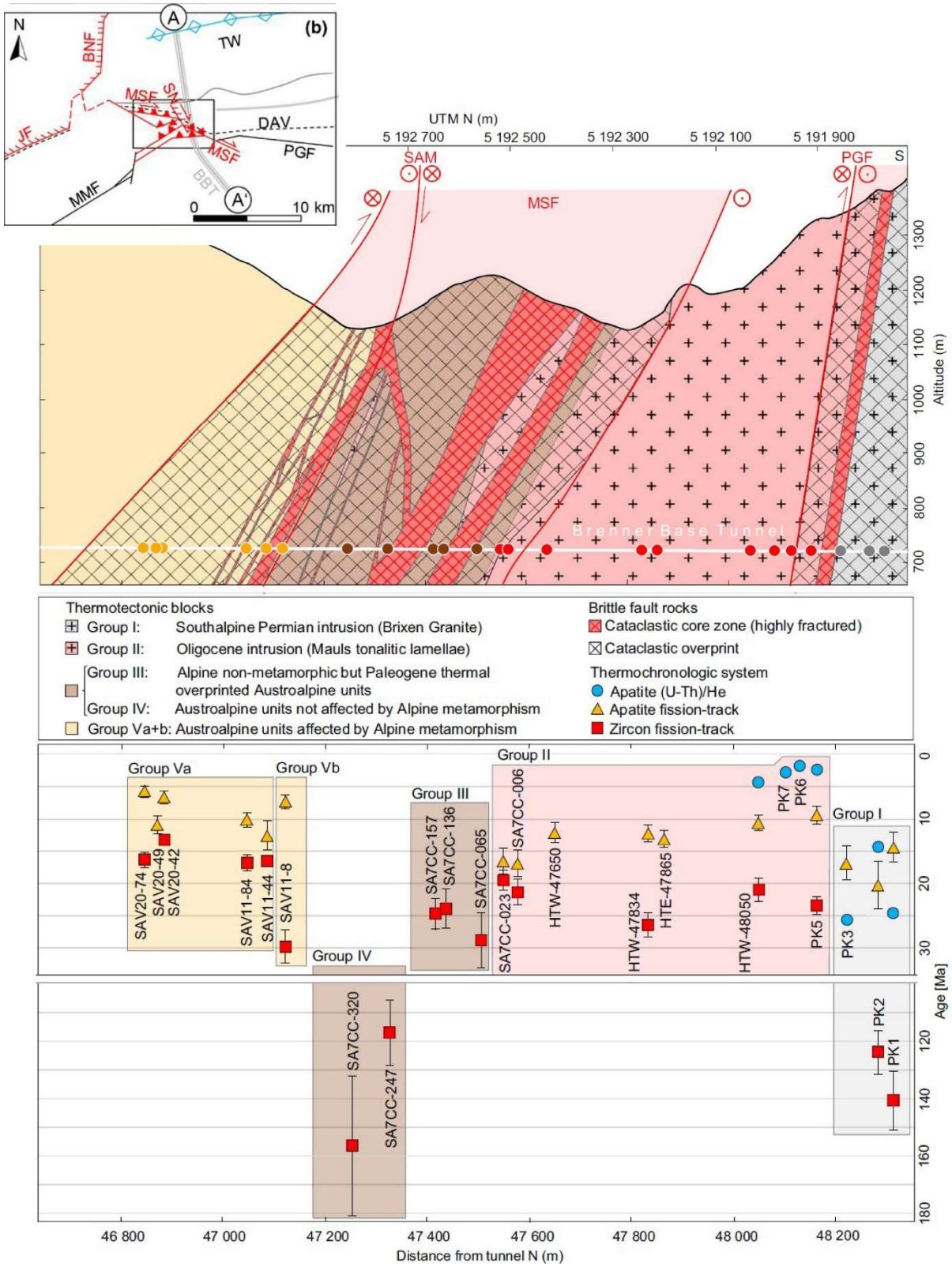

Figure 2.11: Location of the Brenner Base Tunnel, analyzed samples and age data. Ordinate axis Age [Ma] is plotted in two sections due to lack of ages between 35 and 100 Ma. Not every sample contained crystals suitable for all applied dating techniques (ZFT, AFT, AHe) and modelling of thermal histories (Klotz et al. 2019).

Day 3 (Saturday 2nd September)

The Tauern Window and the Brenner Normal Fault

We will take the bus to S. Giacomo (Vizze Valley) and then the minibus to the Vizze mountain hut (2276 m), near Vizze Pass. We will walk around to observe the Upper Permian-Mesozoic metasedimentary cover succession of the distal European margin (Penninic domain) and the contact with the former Lower Permian intrusives now forming the "Zentralgneiss". After lunch, we will descend along a mountain path towards S. Giacomo (elevation loss 480 m) to observe a panoramic view of the structure of the western Tauern Window. Back to the bus, we will have additional stops along the Vizze Valley to discuss the complex kilometer-scale structure of the Tauern Window and the role of the Brenner Fault during Cenozoic exhumation. A final stop in the Fleres Valley, in the hanging wall of the Brenner Fault to observe the locality where the French geologist Déodat Dolomieu discovered in 1789 the Ca-Mg carbonate $CaMg(CO_3)_2$ referred to as Dolomite since then.

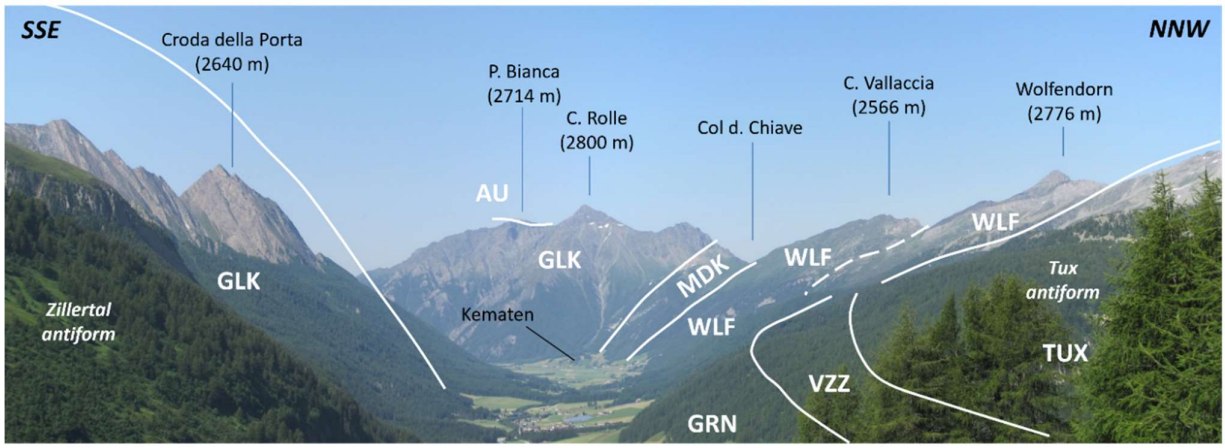

Figure 3.1: View of the Vizze Valley with the Zillertal (on the left) and Tux (on the right) antiforms of the Tauern Window. Fold axes of the two antiforms plunge to the west, therefore the Zentralgneiss is covered to the west by calcschists and ophiolites of the Glockner unit. Acronyms: AU= Austroalpine; GLK= Glockner unit; GRN= Greiner unit (garnet-graphite schist); MDK= Modereck unit; VZZ= Vizze unit; WLF= Wolfendorn unit.

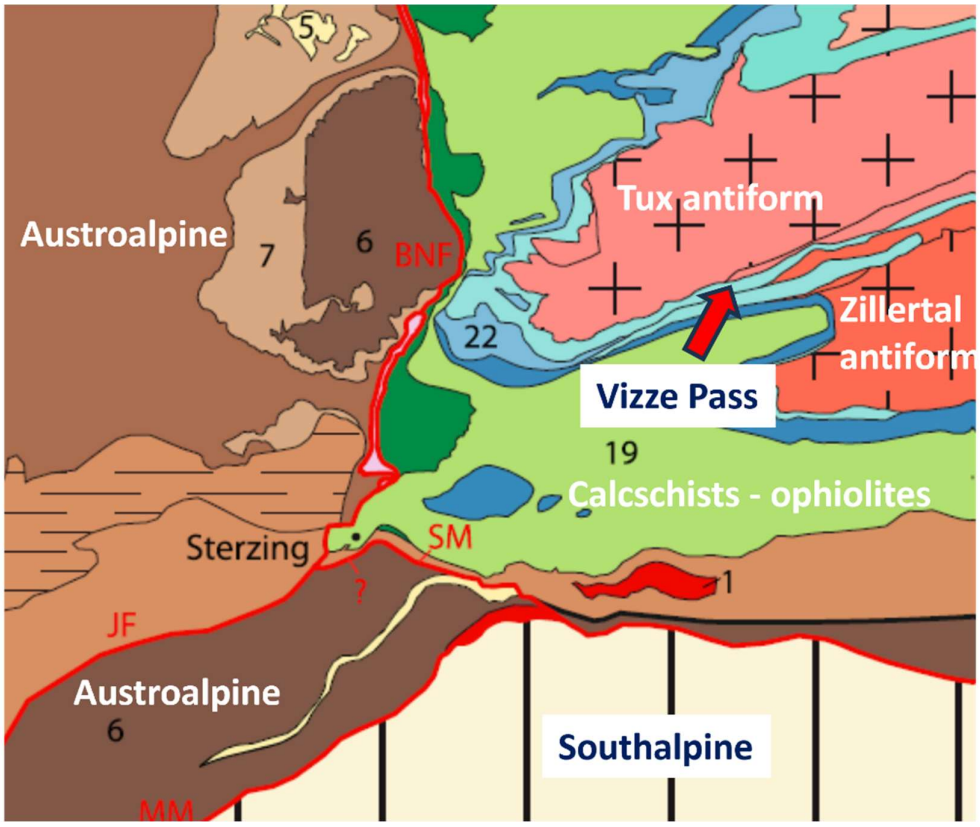

Figure 3.2: Tectonic sketch map of the Vizze Pass area showing the western Tauern Window and the Brenner Normal Fault (BNF) (Schmid et al. 2013).

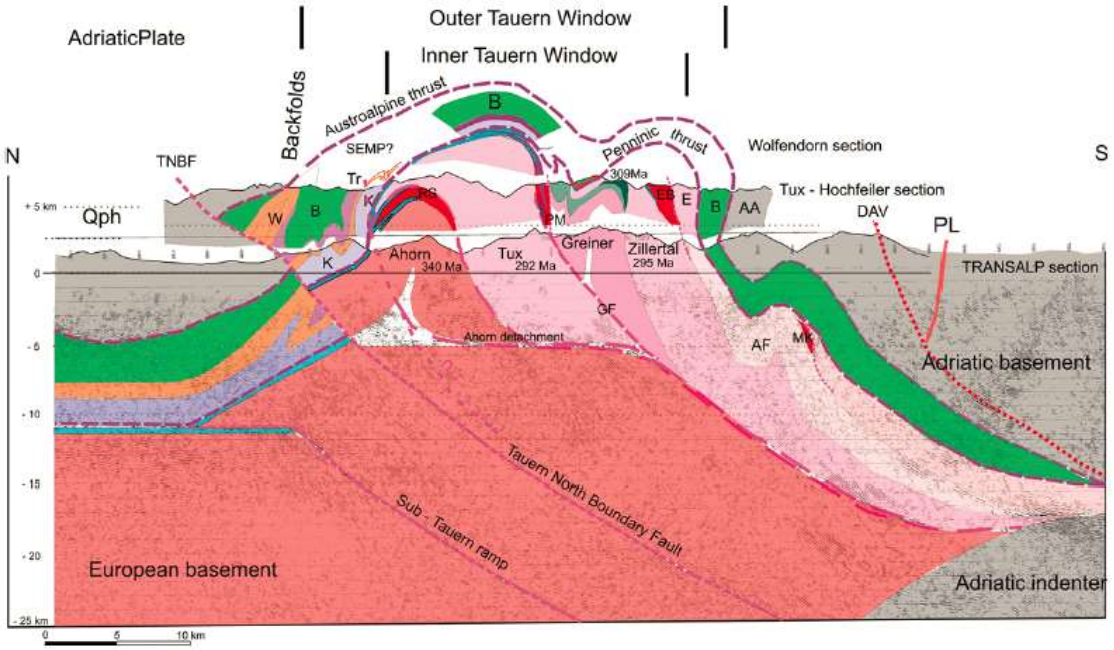

Figure 3.3: Crustal-scale structure of the Tauern Window along the TRANSALP seismic profile according to Lammerer et al. (2011). Note that the deep structure of the region is still debated.

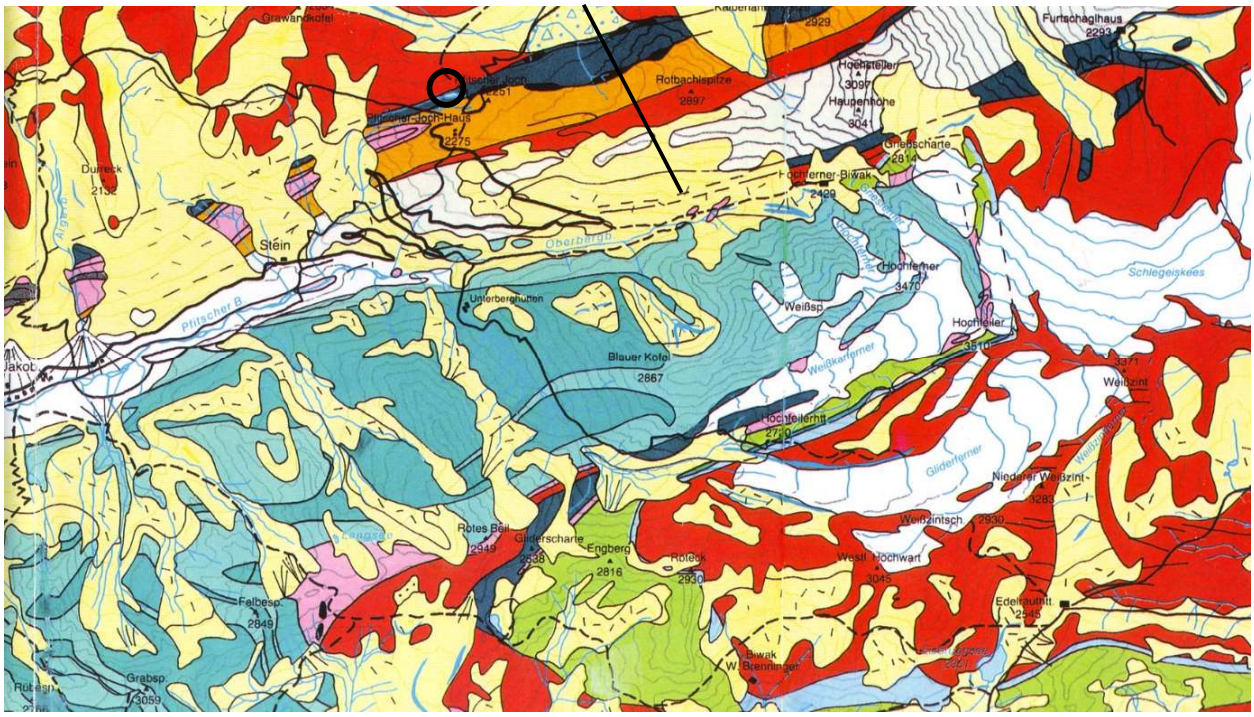

Figure 3.4: Geological map of the upper Vizze (Pfitsch) Valley after Lammerer (1988). Vizze Pass is located on the orange unit including micaschists, metaconglomerates, metarhyolites and garnet-bearing phyllites derived from Upper Carboniferous – Lower Permian sediments of the European plate. The pink unit consists of epidote-ankerite bearing schists, calcitic and dolomitic marbles (often with "cargneule"), and kyanite-bearing quartzites (Upper Permian - Lower Triassic).

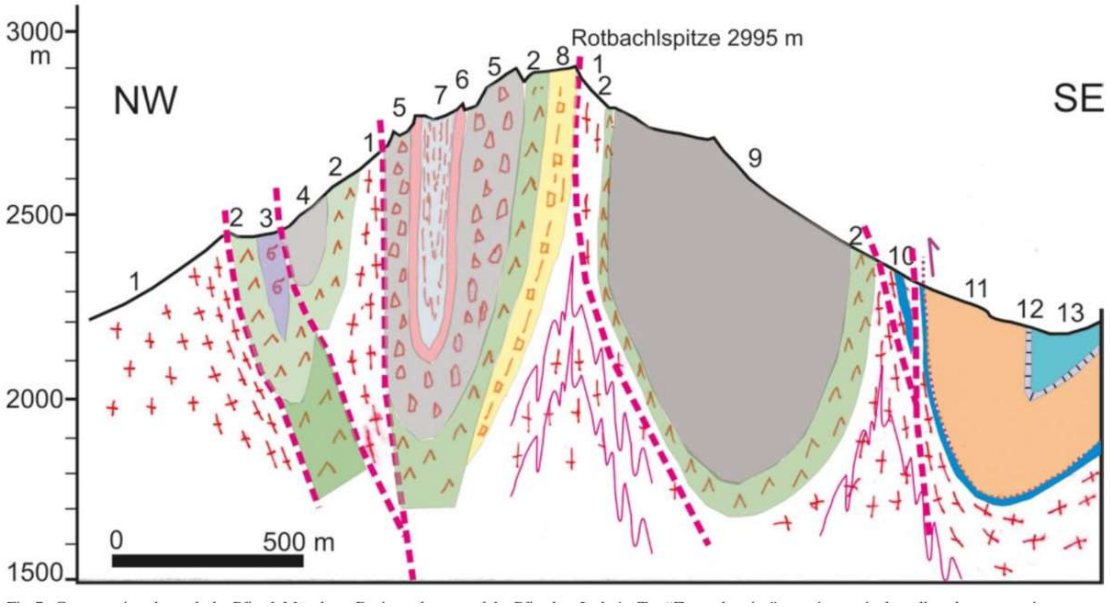

Figure 3.5: NW-SE geological cross section of the Vizze unit (Carboniferous-Triassic), see location in fig. 3.4 (Vesela et al., 2008).

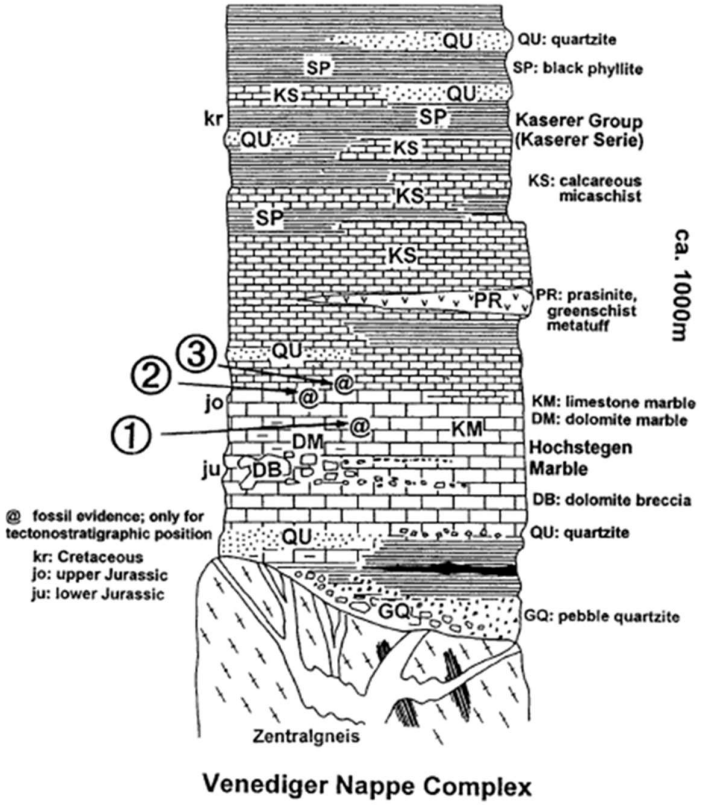

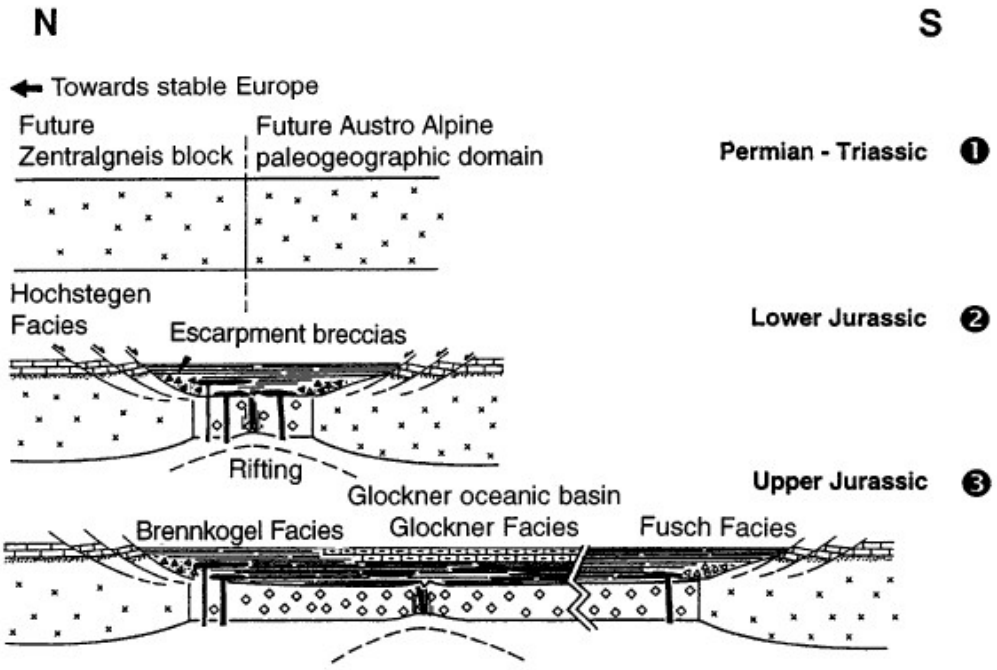

Figure 3.6: Stratigraphic column of the Penninic cover sequence on the northern side of the Vizze Valley, and possible evolution of passive margins of the Alpine Tethys oceanic basin in the future Eastern Alps (from Kurz et al., 1998).

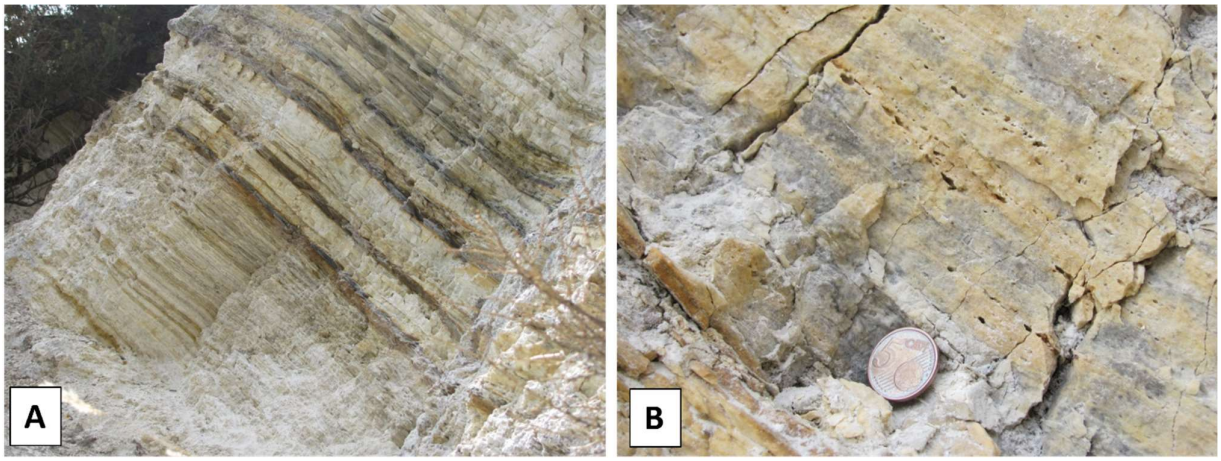

Figure 3.7: Banded calcitic and dolomitic marbles derived from Lower Triassic carbonates of the Vizze unit.

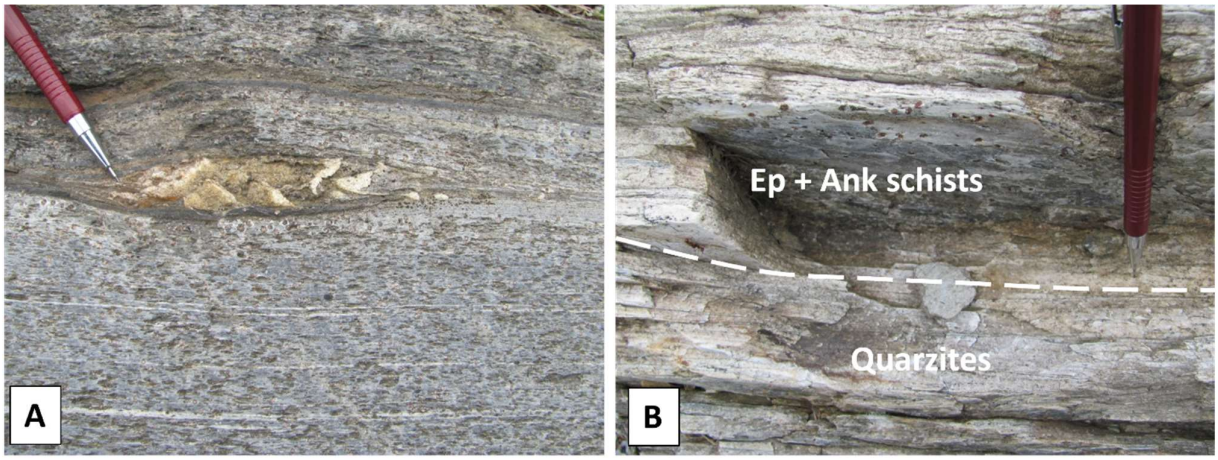

Figure 3.8: Epidote- Ankerite schists (A) and quartzites (B) of the Vizze unit.

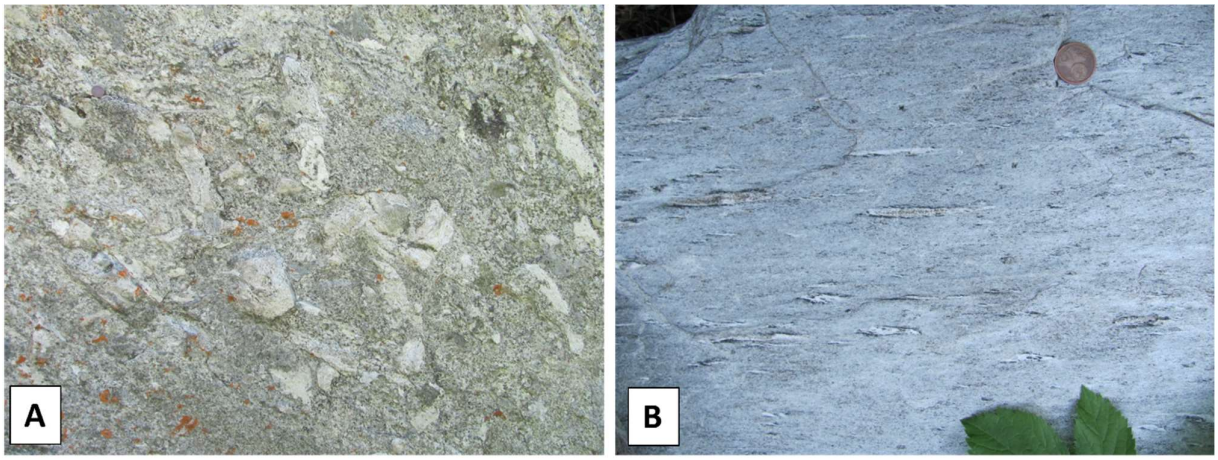

Figure 3.9: Metaconglomerates (A) and Epidote-Ankerite schists (B) with calcitic lenses.

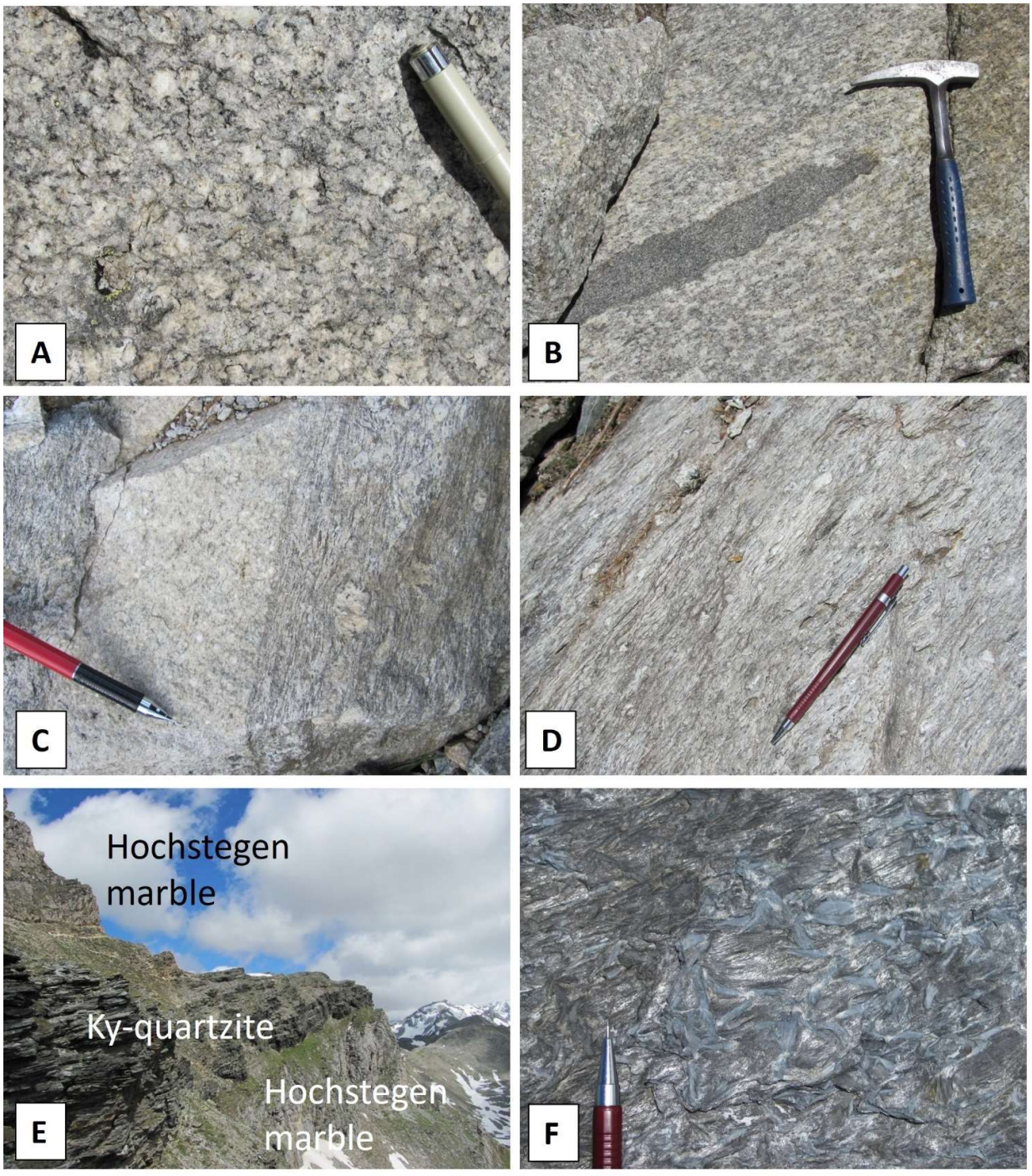

Figure 3.10: A) Granitoid orthogneiss ("Zentralgneiss") preserving the magmatic texture, Penninic domain, Tauern Window. B) The same orthogneiss with a mafic enclave and a well-developed foliation. C) Aplitic dike within the orthogneiss. D) Mylonites after orthogneiss developed at the contact with the hosting basement rocks at Vizze pass, Penninic domain. E) The Hochstegen marble and the kyanite bearing quartzites ("Rhaetizit Quartzite") of the Mesozoic cover of the Tauern Window, Penninic domain. F) Light blue kyanite crystals in the quartzites of fig. (E).

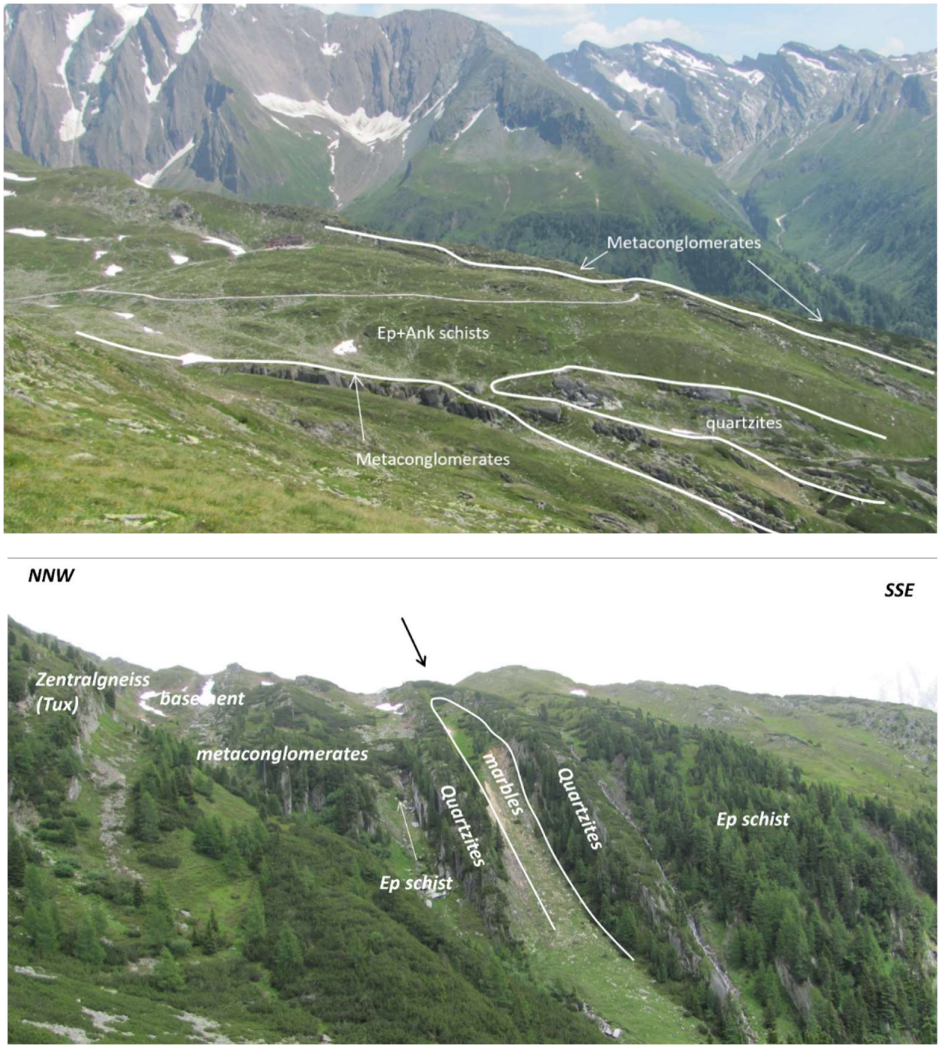

Figure 3.11: Lithological repetitions due to folding inside the Vizze unit, as seen looking E from the path and looking NE from the parking place.

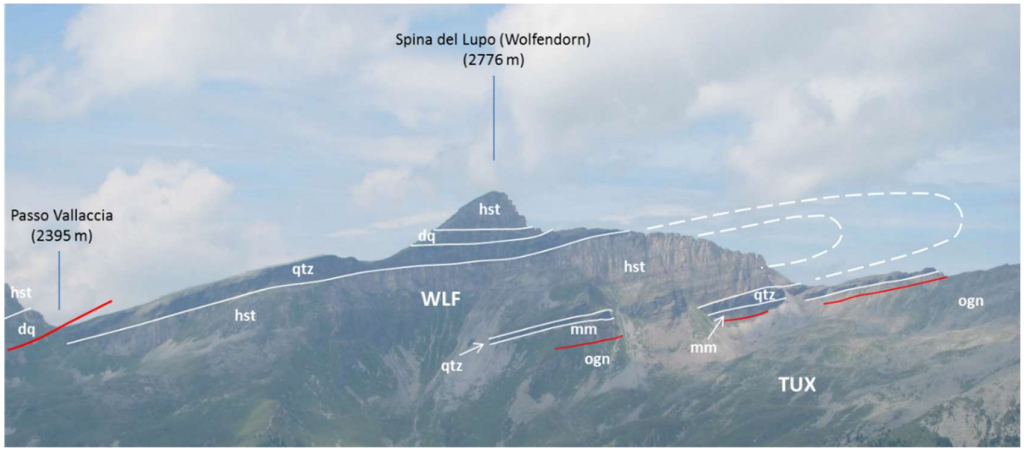

Figure 3.12: View of the Wolfendorn fold from Kematen. Kyanite-Graphite bearing quartzite (*Rhaetizit* Auct., qtz) highlights an isoclinal fold with a N-S trending axis, resting on the orthogneiss (ogn) of the Tux antiform. TUX: Tux antiform; WLF: Wolfendorn unit; hst: Hochstegen marble (Jurassic); qtz: rhaetizit quartzites; dq: quartzites and marbles; mm: calcitic marbles.

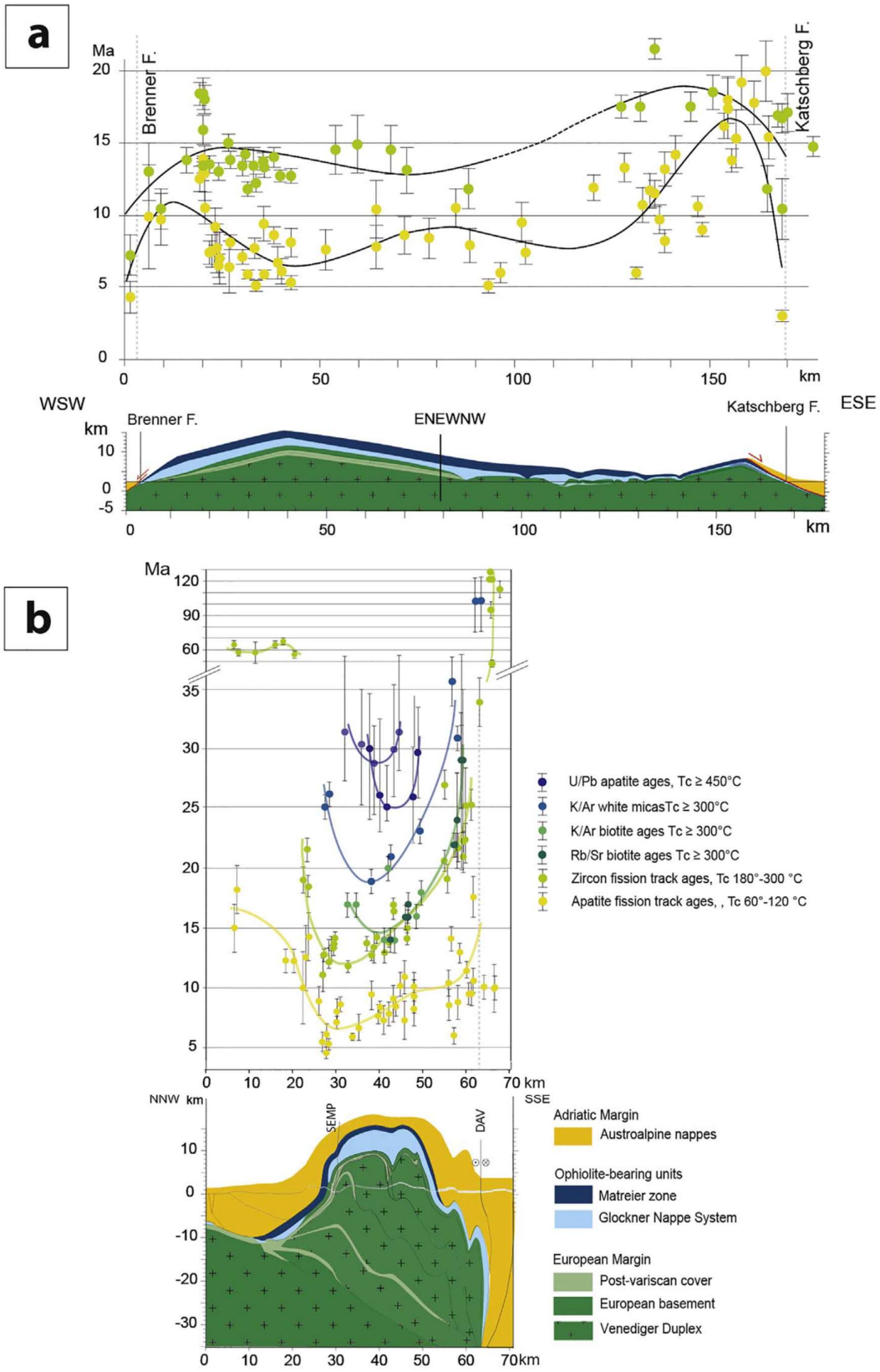

Figure 3.13: Cooling ages projected along an orogen-parallel (a) and an orogen-perpendicular (b) cross-section of the Tauern window, based on the compilation of Bertrand et al. (2017), Most (2003), and Schneider et al. (2015) (from Rosenberg et al., 2018).

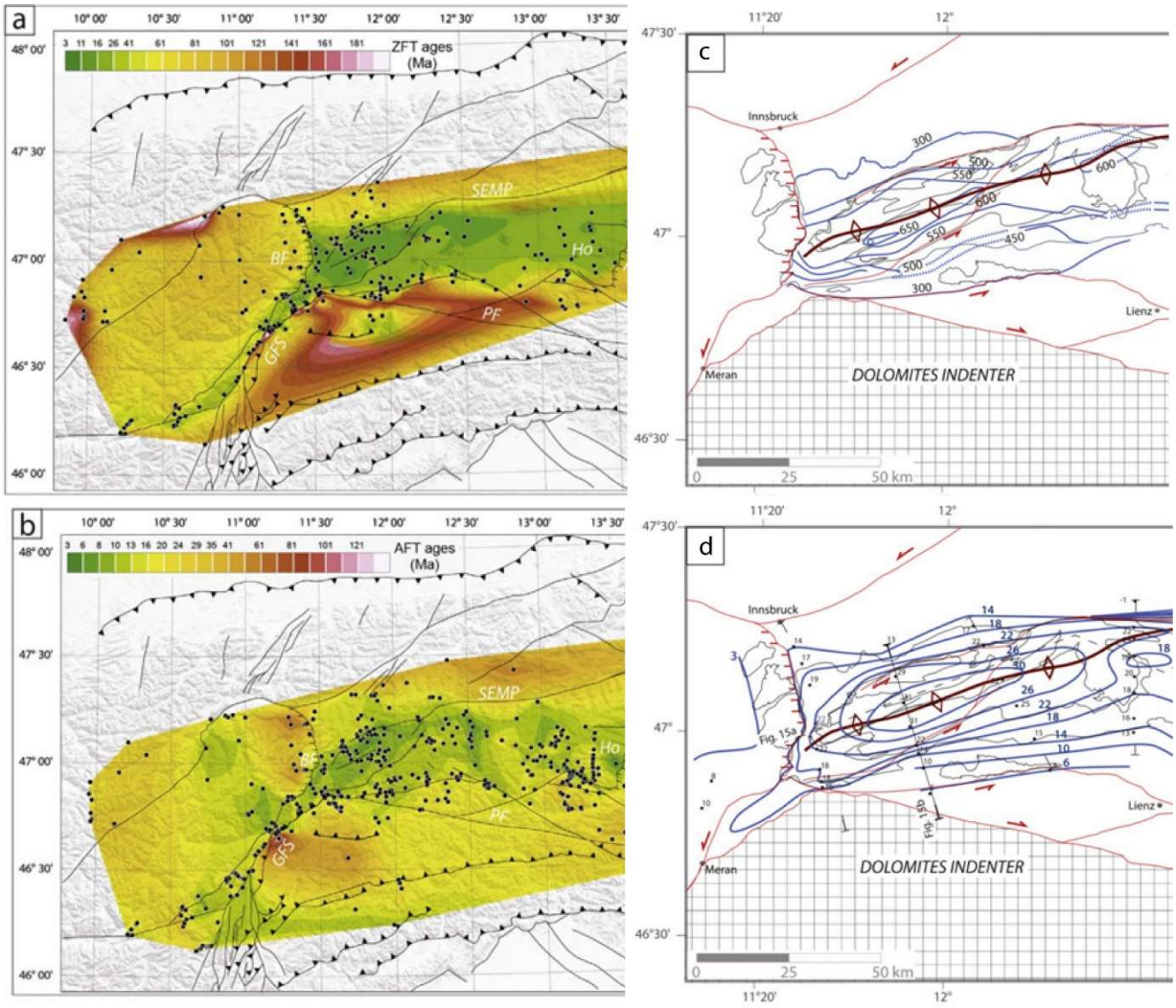

Figure 3.14: a) ZFT ages around the Tauern Window. b) AFT ages. c) Iso-temperature contours of Barrovian metamorphism, numbers indicate metamorphic temperature. d) Comparison with the Tauern dome geometry. Note the different color scales in a) and b). BF: Brenner Fault; GFS: Giudicarie Fault System; KF: Katschberg Fault; PF: Periadriatic Fault; SEMP: Salzach-Ennstal-Mariazell-Puchberg Fault. Ho: Hochalm Dome (after Rosenberg et al., 2018).

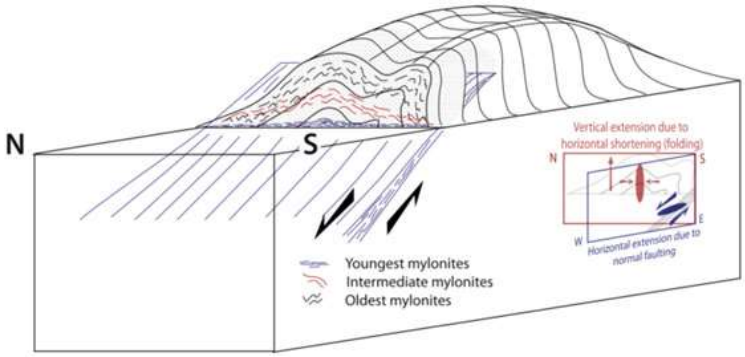

Figure 3.15: 3D model by Rosenberg et al. (2018) showing shortening by folding coeval with extension by normal shearing. Folded mylonites are deactivated and cut by newly formed mylonites that continue to accommodate E-W extension, before they become folded themselves and cut by new mylonites.

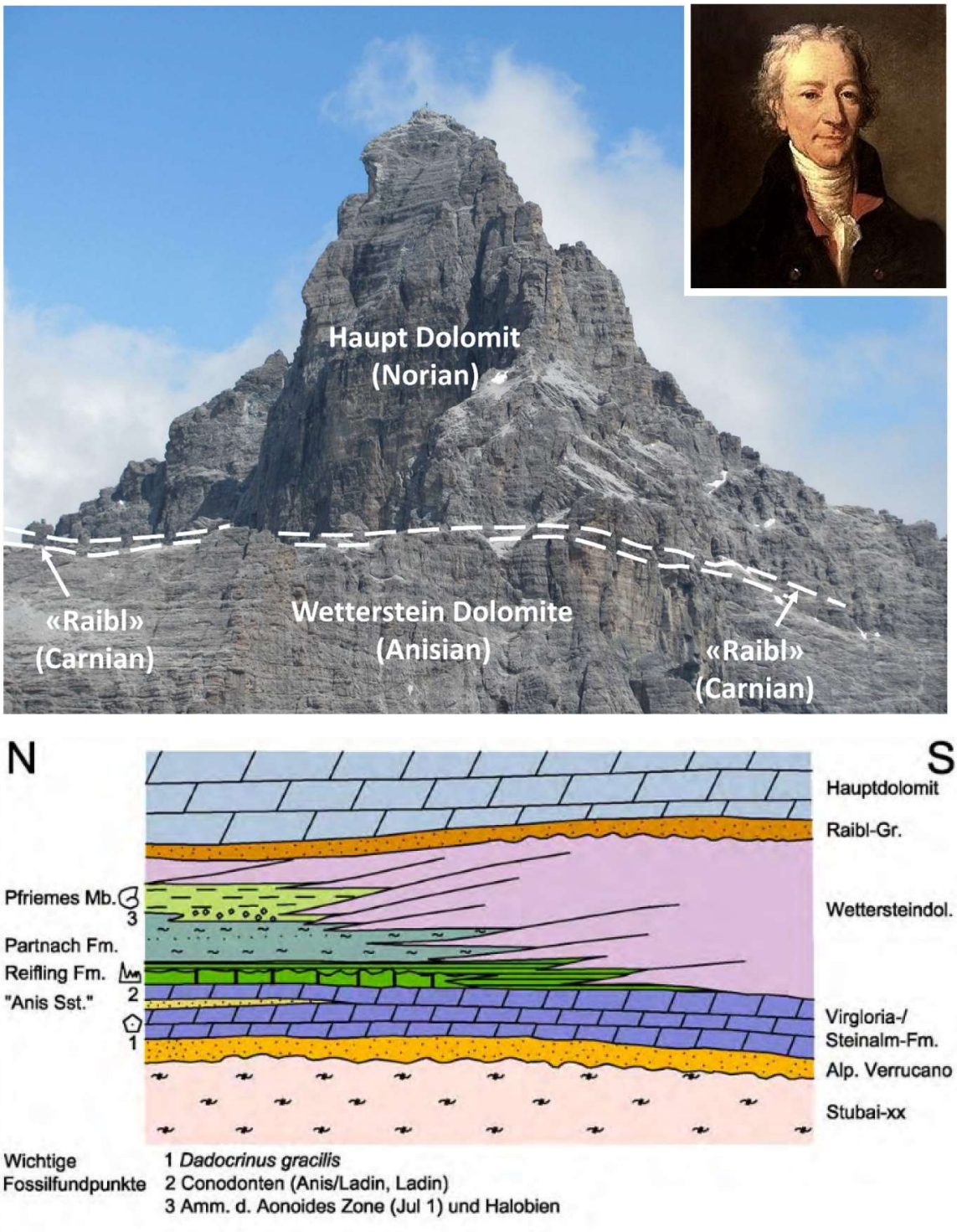

Figure 3.16: Top: The SW face of the Tribulaun (3097 m) in the Fleres Valley, and portrait of Déodat Dolomieu (1750-1801), the famous French geologist who visited this locality and first discovered the existence of $CaMg(CO_3)_2$ (dolomite) in 1789. Bottom: Stratigraphic succession of the so-called "Brenner Mesozoikum", i.e. the post-Variscan autochthonous sedimentary cover of the Austroalpine basement of the Eastern Alps (Brandner et al., 2003).

Day 4 (Sunday 3rd September)

The Southalpine domain of the western Dolomites

The bus will take us to the famous Sella Pass (ca 2180 m a.s.l.). From there, a short walk (about 4 km round trip, 250 m elevation gain) on the path that leads to the Friedrich August mountain hut (ca 2300 m a.s.l.) while enjoying fantastic views of the world-famous western Dolomites carbonate platforms (Sass Pordoi, Marmolada and Sasso Lungo). Along the path we will observe the relationships between the carbonate platforms and the volcanic to volcaniclastic successions of the Southalpine domain. We will have lunch near the hut and then return after lunch to Riva del Garda in time for the ice breaker party, scheduled for 6.30 pm at the venue of the congress.

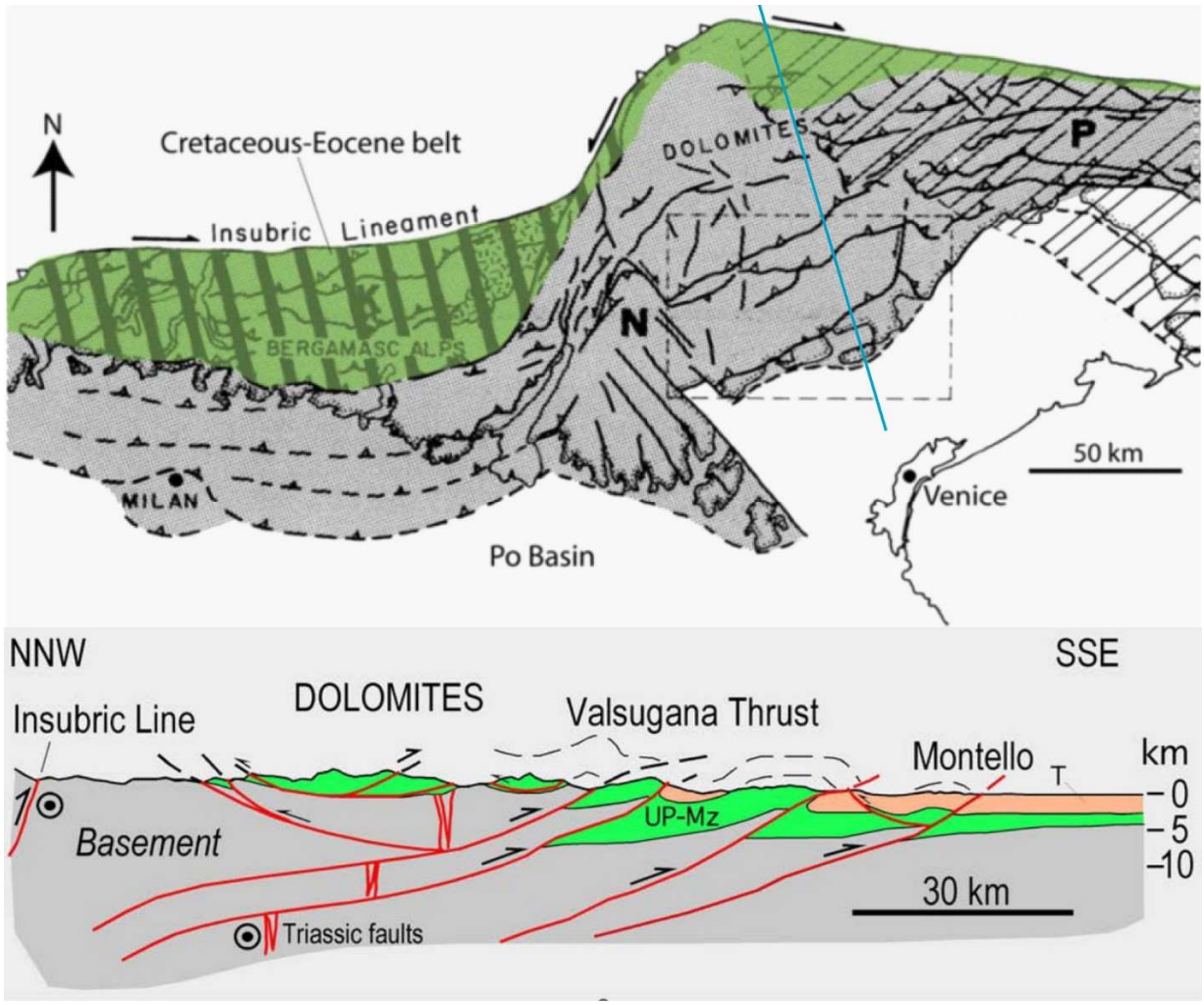

Figure 4.1: Top: The Southern Alps underwent shortening at different times in different areas: green area = Late Cretaceous-Paleogene shortening; P = Paleogene-Early Neogene Dinaric shortening; N = Paleogene-Neogene SSE-vergent shortening in the Southalpine thrust belt. Bottom: cross-section along the southern segment of the Transalp profile (from Doglioni and Carminati 2008).

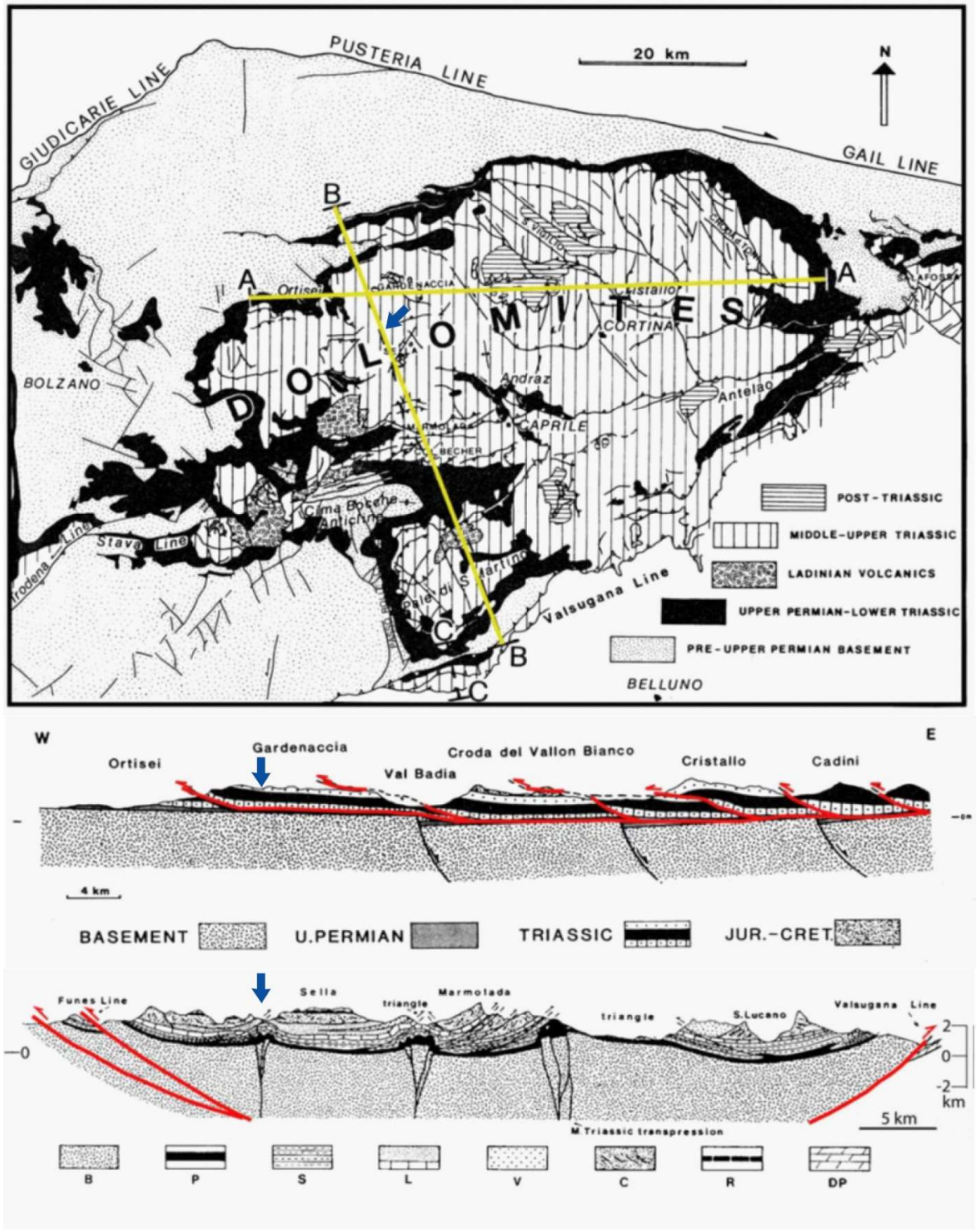

Figure 4.2: Simplified tectonic map of the Dolomites, E-W cross-section showing WSW-vergence of thrusting, and NNW-SSE cross-section showing a wide basement syncline. The blue arrow marks Sella Pass (from Doglioni and Carminati 2008).

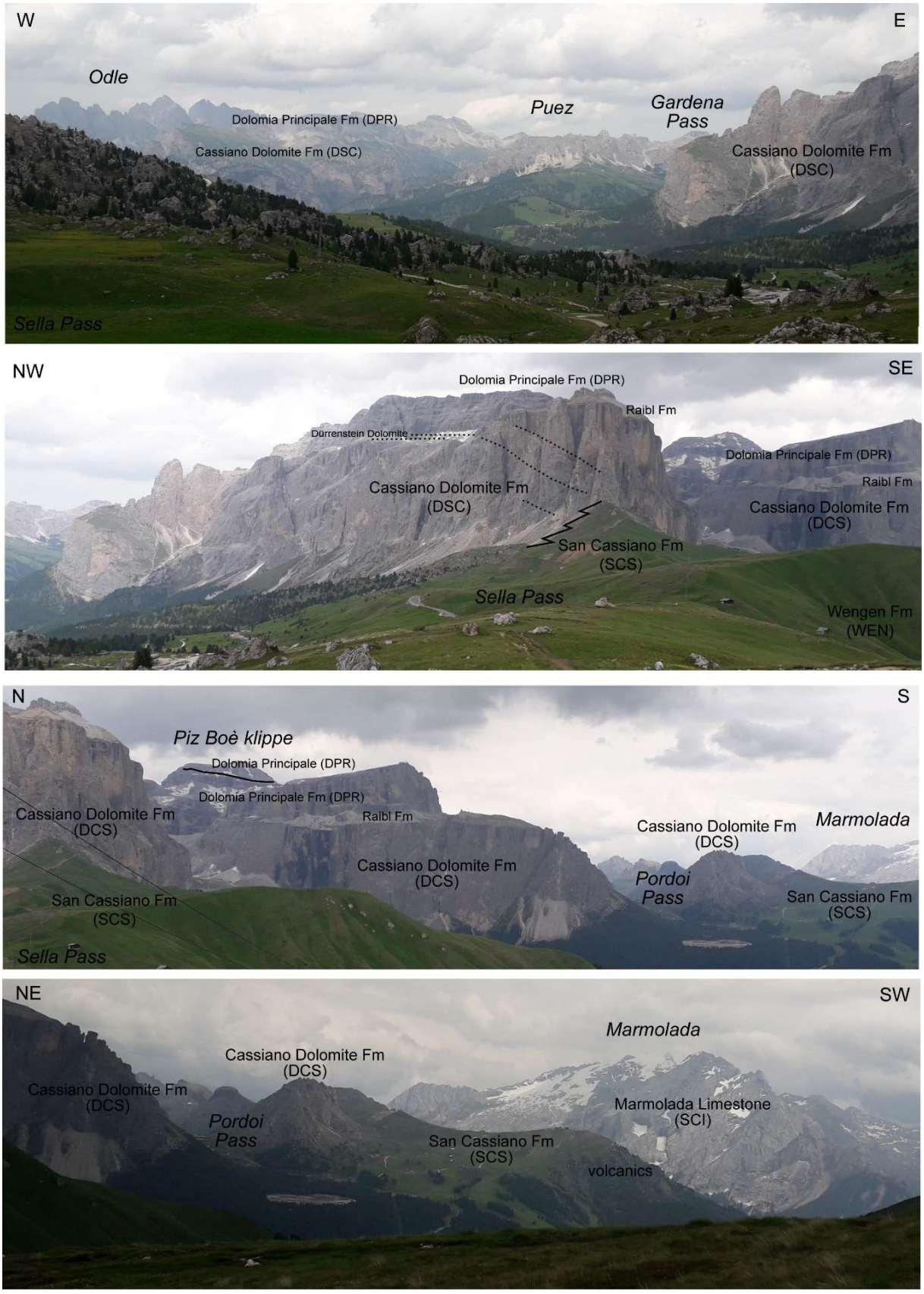

Figure 4.3: Main geological features in the landscape around the Sella Pass

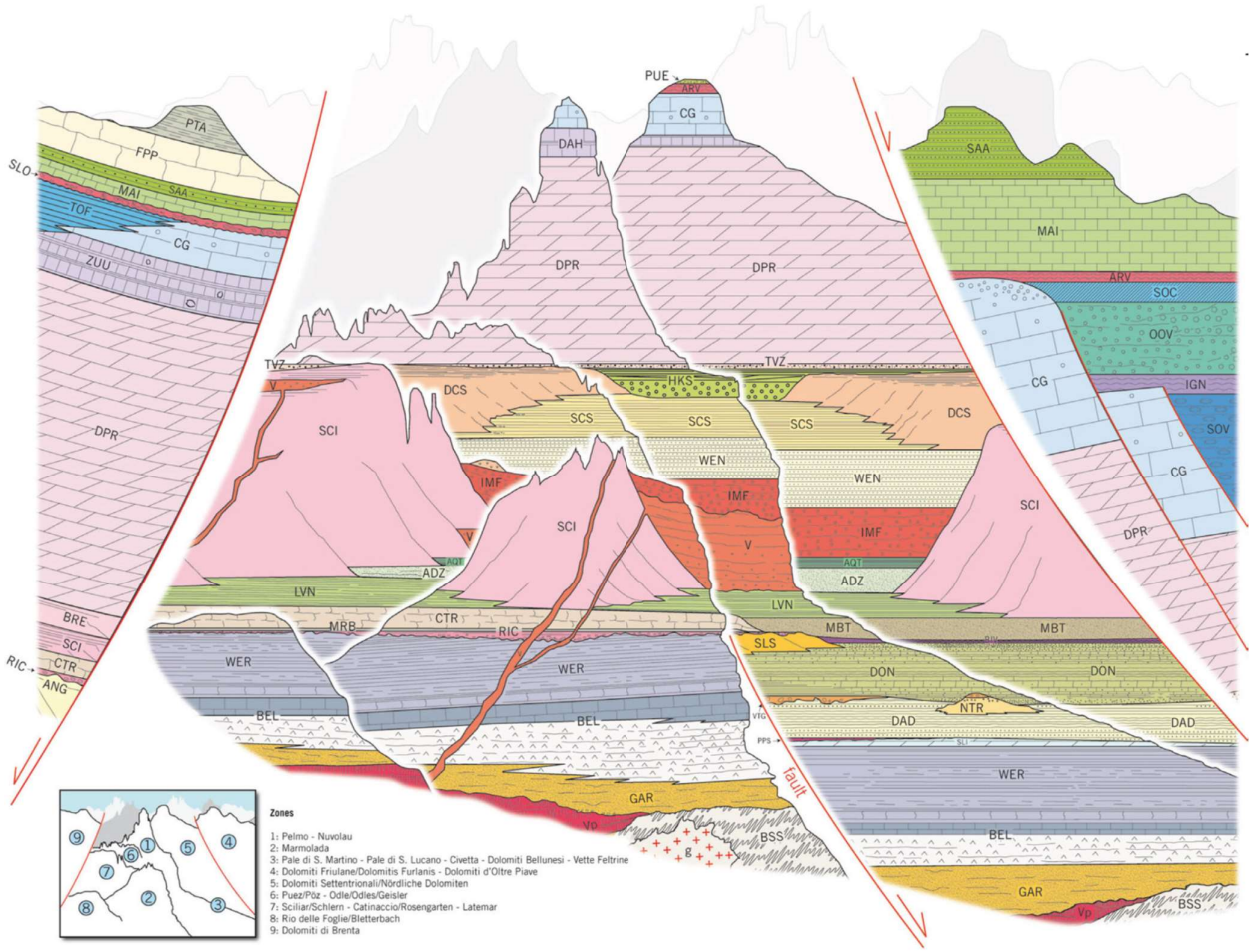
PUE
ARV
CG
DAH
DPR
SAA
MAI
SOC
OOV
IGN
SOV
TVZ
DCS
SCS
HKS
WEN
IMF
SCI
AQT
ADZ
LVN
MRB
CTR
RIC
MBT
SLS
DON
NTR
DAD
WER
BEL
GAR
VD
Vp
BSS
fault
PTA
FPP
TOF
ZUU
BRE
ANG
SLO
Zones
1: Pelmo - Nuvolau
2: Marmolada
3: Pale di S. Martino - Pale di S. Lucano - Civetta - Dolomiti Bellunesi - Vette Feltrine
4: Dolomiti Friulane/Dolomitis Furlanis - Dolomiti d'Oltre Piave
5: Dolomiti Settentrionali/Nördliche Dolomiten
6: Puez/Púz - Odle/Odles/Geisler
7: Sciliar/Schlern - Catinaccio/Rosengarten - Latemar
8: Rio delle Foglie/Bletterbach
9: Dolomiti di Brenta

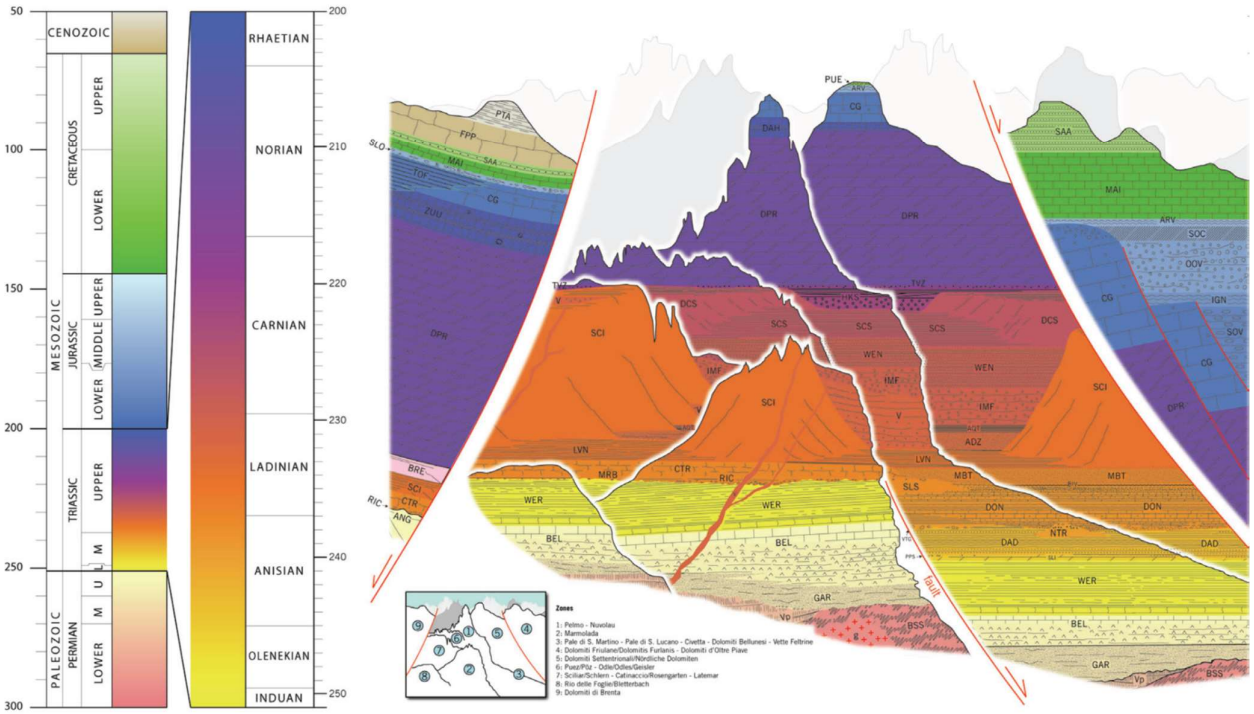
CENOZOIC
MESOZOIC
PALEOZOIC
CRETACEOUS
JURASSIC
TRIASSIC
PERMIAN
UPPER
LOWER
MIDDLE
M
U
L
RHAETIAN
NORIAN
CARNIAN
LADINIAN
ANISIAN
OLENEKIAN
INDUAN
50
100
150
200
250
300
200
210
220
230
240
250

Figure 4.4: Previous page: Lithostratigraphy (top) and chronostratigraphy (bottom) of the Dolomites (from Gianolla et al., 2010). BSS: Metamorphic basement; g: Granitoids; Vp: Permian porphyries; GAR: Val Gardena Sds; BEL: Bellerophon Fm; WER: Werfen Fm; LSI: Lower Serla Dm; PPS: Piz da Peres Cgm; DAD: Gracilis Fm; NTR: Mt. Rite Fm; VTG: Voltago Cgm; SLS: Upper Serla Dm; DON: Dont Fm; RIC: Richthofen Cgm; MRB: Morbiac Fm; CTR: Contrin Lms; BIV: Mt. Bivera Fm; MBT: Ambata Fm; SCI: Sciliar Fm; LVN: Livinallongo/Buchenstein Fm; V: Ladinian volcanics; ADZ: Zoppè Sds; AQT: Aquatona Fm; IMF: Mt. Fernazza Fm; WEN: Wengen Fm; DCS: Cassian Dm; SCS: San Cassiano Fm; HKS: Heiligkreutz Fm; TVZ: Travenanzes Fm; DPR: Dolomia Principale; DAH: Dachstein Lms; CG: Calcari Grigi; ARV: Ammonitico Rosso Veronese; PUE: Puez Marls.

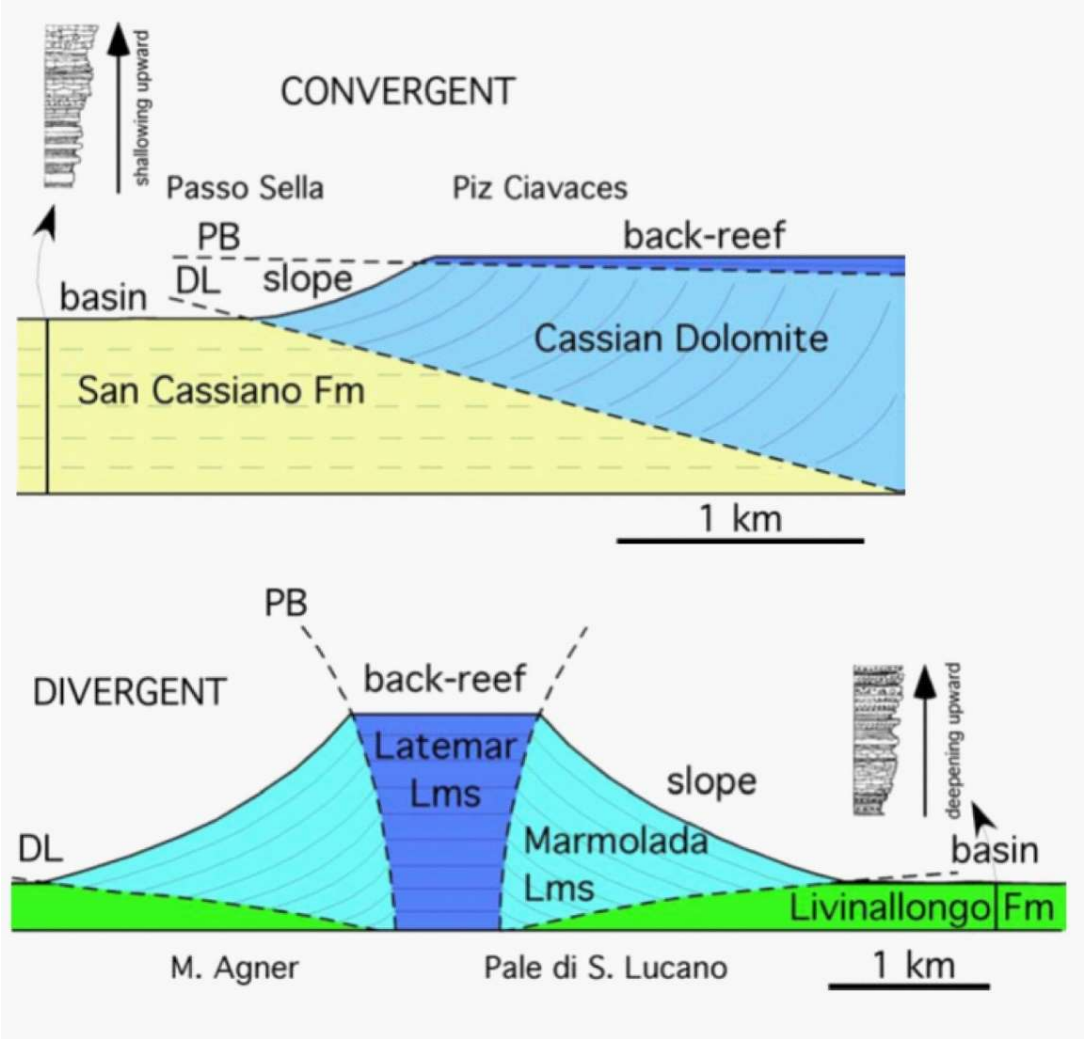

Figure 4.5: Top: The western margin of the Sella Carnian carbonate platform (Upper Cassian Dolomite) provides an example of convergence between the platform break plane (PB) and the downlap plane (DL). The coeval basin (San Cassiano Formation) consequently shows a shallowing upward sequence. The flat and gentle dip of the platform break indicates negligible subsidence rate. Bottom: The Ladinian Pale di San Lucano platform provides an example of divergent platform break (PB) and downlap (DP) planes. The basinal Livinallongo Formation shows a deepening upward sequence. The steep platform break is controlled by fast subsidence rate, which cannot be generated only by sea-level rise since the platform sequence is thicker than 1 km (from Doglioni and Bosellini, 1989; Doglioni and Carminati 2008).

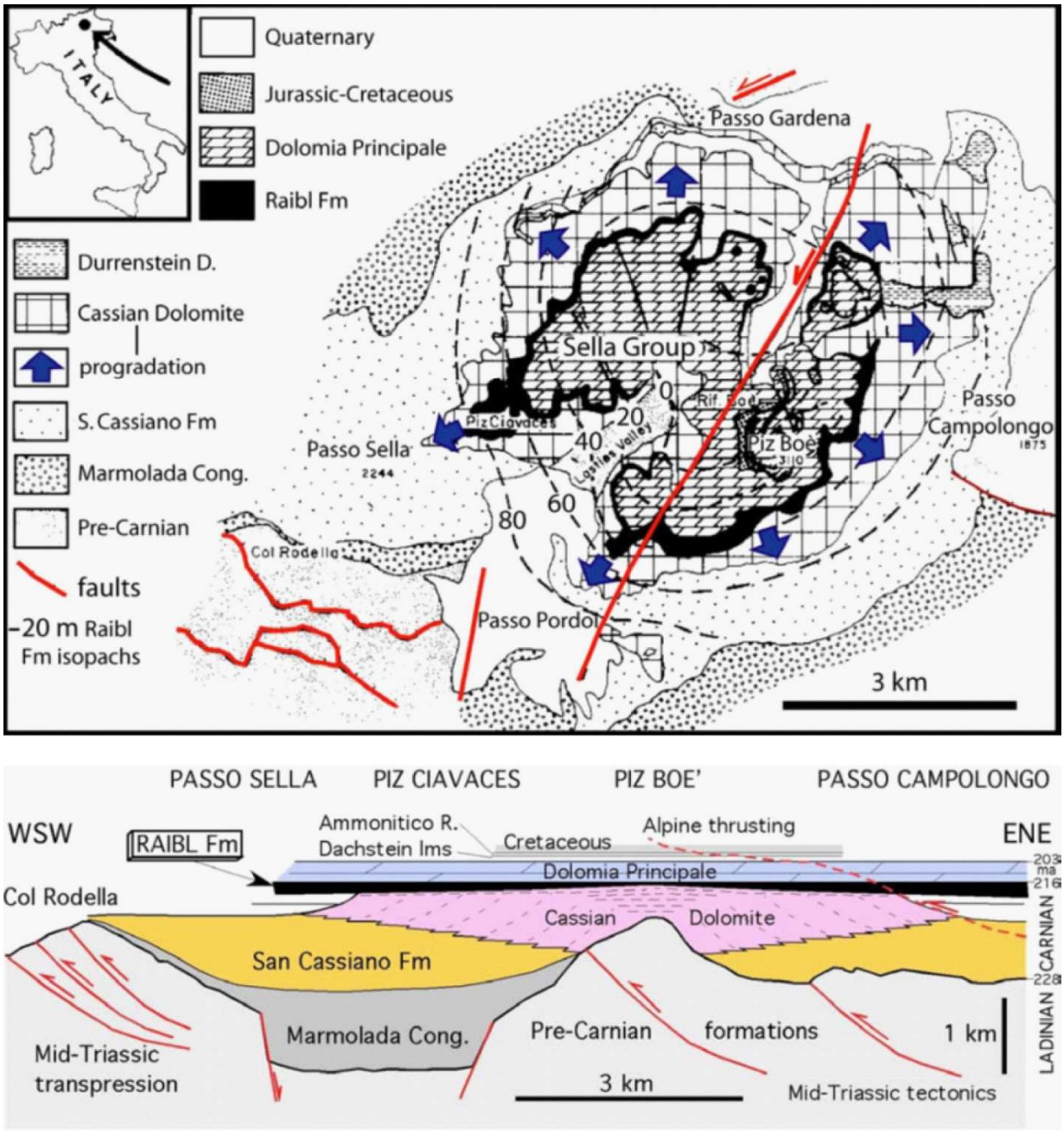

Figure 4.6: Simplified geological map and cross section of the Sella Group, a perfectly preserved atoll (Leonardi, 1967). Notice the radial progradation of the Carnian carbonate platform (Cassian Dolomite). The isopachs of the Raibl Fm indicate a thickening of the formation away from the Carnian platform. This suggests that the compaction of the Cassian basinal deposits generated the subsidence that allowed the deposition of the Raibl Fm (from Doglioni and Goldhammer 1988; Doglioni and Carminati 2008).

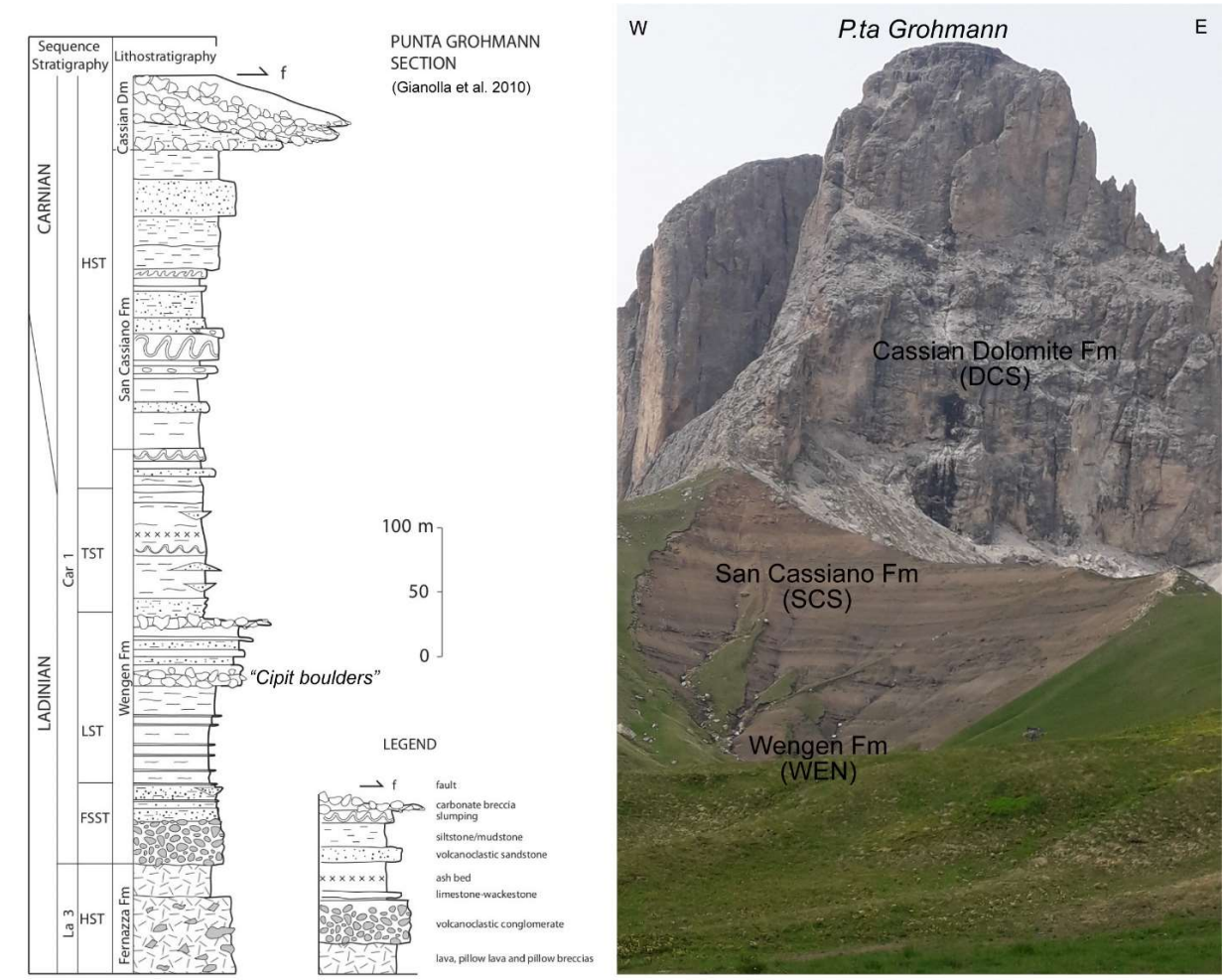

Figure 4.7: Schematic log (left) and view (right) of the Punta Grohmann section (from Gianolla et al 2010). Below, an example of "Cipit boulder"

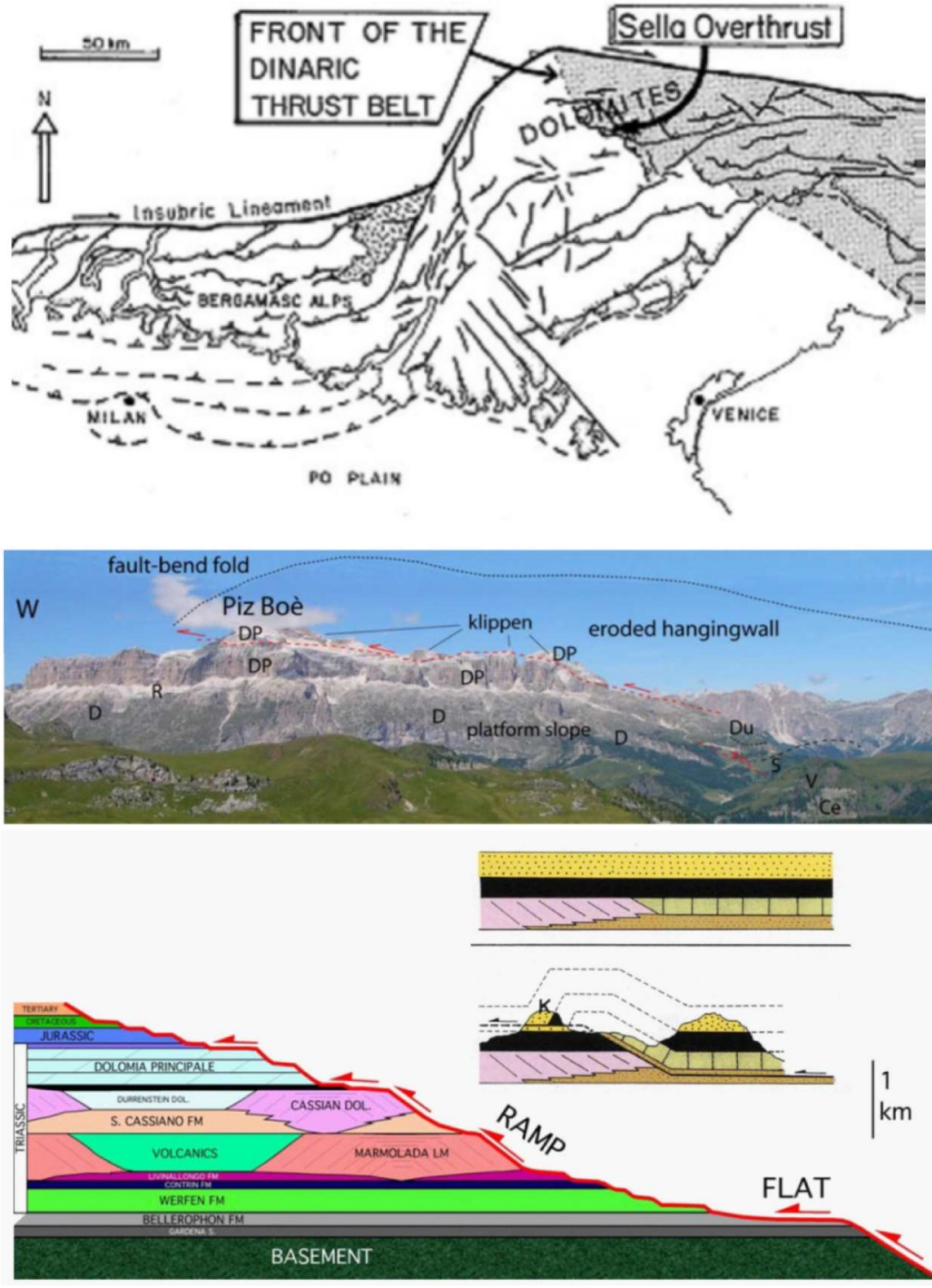

Figure 4.8: The Sella thrust as front of the Paleogene - early Neogene WSW-vergent Dinaric thrust belt, and potential control of the stratigraphic succession on the localization of ramps and flats (from Doglioni and Carminati 2008). The klippen (K) of the Dolomites are interpreted as remaining parts of the hanging-wall of thrust faults like that shown in this figure.

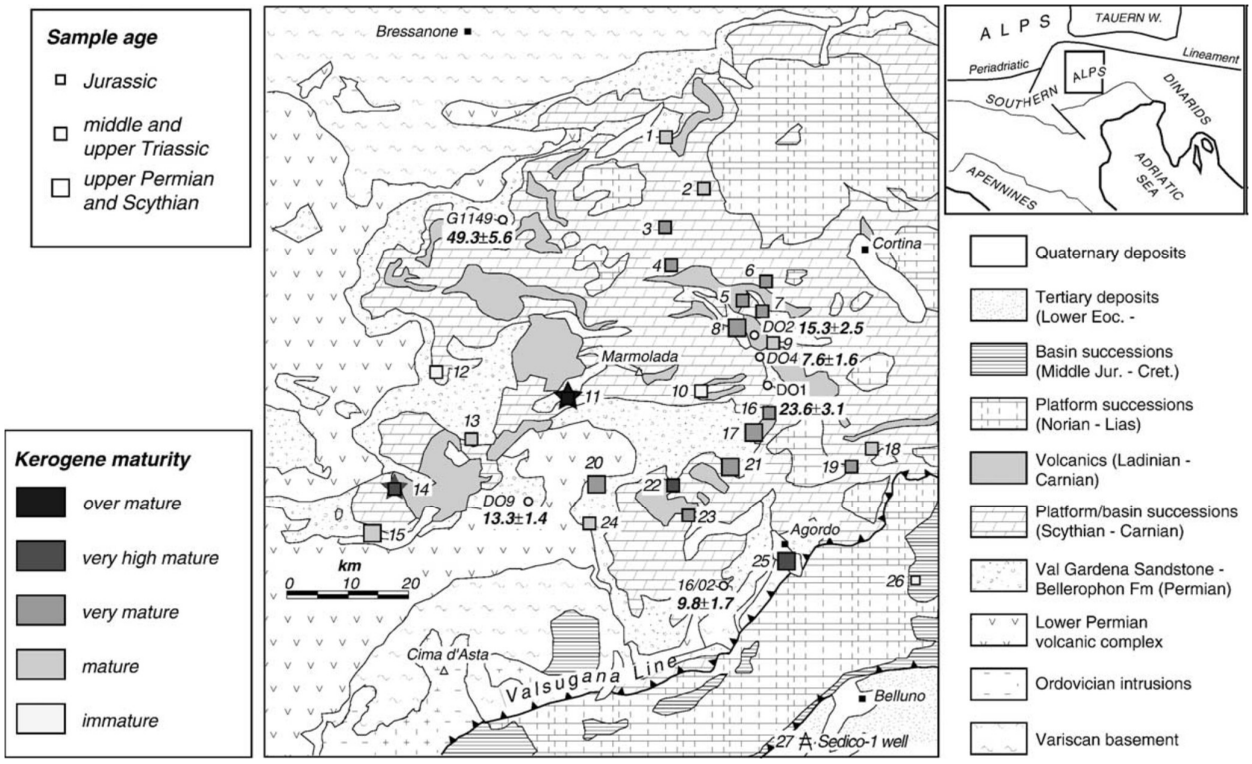

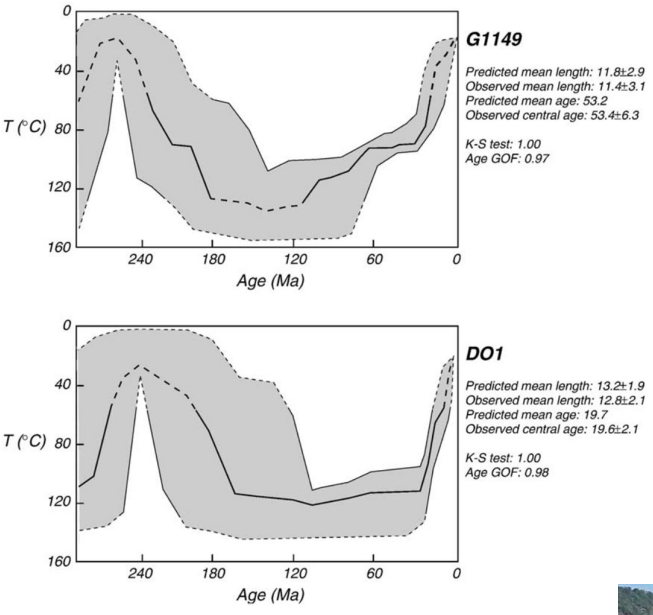

Figure 4.9: Map of the studied area with location of organic matter maturity and fission-track data. Stars indicate data affected by local thermal perturbations due to Ladinian dykes. Italic numbers indicate localities sampled for organic matter analysis. Fission-track ages are indicated with bold numbers (bold italic: partially annealed samples). On the left, T-t paths modelled with AFTsolve (from Zattin et al. 2006).

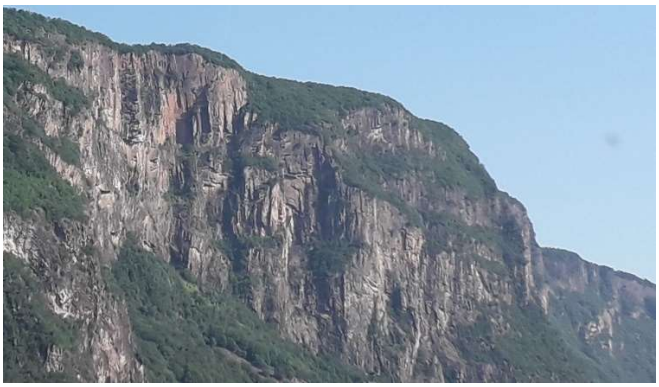

Figure 4.10: Permian volcanics of the Southalpine domain and their cooling joints as seen from the motorway north of Bolzano.

References

Bertotti, G., Picotti, V., Bernoulli, D., & Castellarin, A. (1993). From rifting to drifting: tectonic evolution of the South-Alpine upper crust from the Triassic to the Early Cretaceous. Sedimentary Geology, 86(1-2), 53-76.

Bertrand, A., Rosenberg, C., Rabaute, A., Herman, F., & Fügenschuh, B. (2017). Exhumation mechanisms of the Tauern Window (Eastern Alps) inferred from apatite and zircon fission track thermochronology. Tectonics, 36(2), 207-228.

Brandner, R., Resch, W., & Reiter, F. Das Brennermesozoikum. Sedimentäre Faziesentwicklungen in metamorphen Gesteinen und tektonische Konsequenzen.

Broderick, C., Wotzlaw, J. F., Frick, D. A., Gerdes, A., Ulianov, A., Günther, D., & Schaltegger, U. (2015). Linking the thermal evolution and emplacement history of an upper-crustal pluton to its lower-crustal roots using zircon geochronology and geochemistry (southern Adamello batholith, N. Italy). Contributions to Mineralogy and Petrology, 170, 1-17.

Dewey, J. F., Helman, M. L., Knott, S. D., Turco, E., & Hutton, D. H. W. (1989). Kinematics of the western Mediterranean. Geological Society, London, Special Publications, 45(1), 265-283.

Doglioni, C., & Bosellini, A. (1989). Platform break-downlap planes relationship in prograding carbonates platforms: A tool for the reconstruction of basin evolution. Bollettino della Società geologica italiana, 108(1), 175-182.

Doglioni, C. & E. Carminati (2008) Structural styles and Dolomites field trip. Memorie Descrittive della Carta Geologica d'Italia, 82, 293 pp.

Doglioni, C., & Goldhammer, R. K. (1988). Compaction-induced subsidence in the margin of a carbonate platform. Basin Research, 1(4), 237-246.

Gianolla, P., Avanzini, M., Breda, A., Kustatscher, E., Preto, N., Roghi, G., ... & Stefani, M. (2010). DOLOMITES–7th International Triassic Field Workshop (Pan–European Correlation of the Triassic). Field trip to the UNESCO World Heritage Site of the Tethyan Triassic, 5(10.09), 2010.

Handy, M. R., Schmid, S. M., Bousquet, R., Kissling, E., & Bernoulli, D. (2010). Reconciling plate-tectonic reconstructions of Alpine Tethys with the geological–geophysical record of spreading and subduction in the Alps. Earth-Science Reviews, 102(3-4), 121-158.

Ji, W. Q., Malusà, M. G., Tiepolo, M., Langone, A., Zhao, L., & Wu, F. Y. (2019). Synchronous Periadriatic magmatism in the Western and Central Alps in the absence of slab breakoff. Terra Nova, 31(2), 120-128.

Klotz, T., Pomella, H., Reiser, M., Fügenschuh, B., & Zattin, M. (2019). Differential uplift on the boundary between the Eastern and the Southern European Alps: Thermochronologic constraints from the Brenner Base Tunnel. Terra Nova, 31(3), 281-294.

Kurz, W., Neubauer, F., Genser, J., & Dachs, E. (1998). Alpine geodynamic evolution of passive and active continental margin sequences in the Tauern Window (eastern Alps, Austria, Italy): a review. Geologische rundschau, 87, 225-242.

Lammerer, B. (1988). Thrust-regime and transpression-regime tectonics in the Tauern Window (Eastern Alps). Geologische Rundschau, 77, 143-156.

Lammerer, B., Selverstone, J., & Franz, G. (2011). Field trip to the Tauern Window region along the TRANSALP seismic profile, Eastern Alps, Austria.

Malusà, M. G., Faccenna, C., Baldwin, S. L., Fitzgerald, P. G., Rossetti, F., Balestrieri, M. L., ... & Piromallo, C. (2015). Contrasting styles of (U) HP rock exhumation along the Cenozoic Adria-Europe plate boundary (Western Alps, Calabria, Corsica). Geochemistry, Geophysics, Geosystems, 16(6), 1786-1824.

Malusà, M. G., Guillot, S., Zhao, L., Paul, A., Solarino, S., Dumont, T., ... & Yuan, H. (2021). The deep structure of the Alps based on the CIFALPS seismic experiment: A synthesis. Geochemistry, Geophysics, Geosystems, 22(3), e2020GC009466.

Most, P., Dunkl, I., & Frisch, W. (2003). Fission track tomography of the Tauern Window along the TRANSALP profile. Memorie di Scienze Geologiche, Padova, 54, 225-226.

Piromallo, C., & Morelli, A. (2003). P wave tomography of the mantle under the Alpine-Mediterranean area. Journal of Geophysical Research: Solid Earth, 108(B2).

Rosenberg, C. L., Schneider, S., Scharf, A., Bertrand, A., Hammerschmidt, K., Rabaute, A., & Brun, J. P. (2018). Relating collisional kinematics to exhumation processes in the Eastern Alps. Earth-Science Reviews, 176, 311-344.

Schmid, S. M., Scharf, A., Handy, M. R., & Rosenberg, C. L. (2013). The Tauern Window (Eastern Alps, Austria): a new tectonic map, with cross-sections and a tectonometamorphic synthesis. Swiss Journal of Geosciences, 106(1), 1-32.

Schneider, S., Hammerschmidt, K., Rosenberg, C. L., Gerdes, A., Frei, D., & Bertrand, A. (2015). U–Pb ages of apatite in the western Tauern Window (Eastern Alps): Tracing the onset of collision-related exhumation in the European plate. Earth and Planetary Science Letters, 418, 53-65.

Schoene, B., Schaltegger, U., Brack, P., Latkoczy, C., Stracke, A., & Günther, D. (2012). Rates of magma differentiation and emplacement in a ballooning pluton recorded by U–Pb TIMS-TEA, Adamello batholith, Italy. Earth and Planetary Science Letters, 355, 162-173.

Sun, W., Zhao, L., Malusà, M. G., Guillot, S., & Fu, L. Y. (2019). 3-D Pn tomography reveals continental subduction at the boundaries of the Adriatic microplate in the absence of a precursor oceanic slab. Earth and Planetary Science Letters, 510, 131-141.

Tiepolo, M., Tribuzio, R., Ji, W. Q., Wu, F. Y., & Lustrino, M. (2014). Alpine Tethys closure as revealed by amphibole-rich mafic and ultramafic rocks from the Adamello and the Bergell intrusions (Central Alps). Journal of the Geological Society, 171(6), 793-799.

Veselá, P., Lammerer, B., Wetzel, A., Söllner, F., & Gerdes, A. (2008). Post-Variscan to Early Alpine sedimentary basins in the Tauern window (eastern Alps). Geological Society, London, Special Publications, 298(1), 83-100.

Viola, G., Mancktelow, N. S., & Seward, D. (2001). Late Oligocene-Neogene evolution of Europe-Adria collision: New structural and geochronological evidence from the Giudicarie fault system (Italian Eastern Alps). Tectonics, 20(6), 999-1020.

Winterer, E. L., & Bosellini, A. (1981). Subsidence and sedimentation on Jurassic passive continental margin, Southern Alps, Italy. AAPG bulletin, 65(3), 394-421.

Zanchetta, S., Montemagni, C., Mascandola, C., Mair, V., Morelli, C., & Zanchi, A. (2023). The Meran-Mauls Fault: Tectonic switching from compression to transpression along a restraining bend of the Periadriatic Fault. Journal of Structural Geology, 172, 104878.

Zattin, M., Cuman, A., Fantoni, R., Martin, S., Scotti, P., & Stefani, C. (2006). From Middle Jurassic heating to Neogene cooling: The thermochronological evolution of the southern Alps. Tectonophysics, 414(1-4), 191-202.

Zhao, L., Paul, A., Malusà, M. G., Xu, X., Zheng, T., Solarino, S., ... & Zhu, R. (2016). Continuity of the Alpine slab unraveled by high-resolution P wave tomography. Journal of Geophysical Research: Solid Earth, 121(12), 8720-8737.